A bottom up mechanistic perspective on the nanostructured metallic electrocatalysts for Hydrogen Evolution Reactions (HER)

Jaya Verma[1]* and Saurav Goel[1,2]

[1]School of Engineering, London South Bank University, London, SE1 0 AA, UK
[2] Department of Mechanical Engineering, University of Petroleum and Energy Studies, Dehradun, 248007, India

Corresponding author: jayaverma745@gmail.com

Abstract

In the extant literature, a wide variety of processes for the production of H_2 can be seen but the active, cost-effective and stable metal electrocatalysts for hydrogen evolution reaction (HER) are essential ones to achieve sustainable energy systems. As such, Pt is a widely used electro-catalyst for HER but its cost is significantly higher that what it needs to be. Taking this as the main motivation, in this review, cheap and effective transition metals for cost-effective electrocatalysts for hydrogen evolution reaction were reviewed. On course of this exploration, transition metals such as molybdenum (Mo), tungsten (W) and composites such as reduced graphene oxide-supported PdAu nanoparticles and RuCo alloy nanoparticles embedded into N-Doped carbon were identified as some of the cost-effective electro-catalytic agents for HER. This review adds new insights into the stability and durability studies of these agents as well as prospects of their commercialisation and market readiness level for HER. Finally, a summary of the challenges in the future development of novel processing methodologies is presented which suggested that the artificial photosynthesis can be a very promising area of development.

Keywords: H_2 production, electrocatalysts, electro-catalytic activity, HER, sustainable & clean energy

Abbreviations:

CC	Carbon cloth
CNT	Carbon nanotubes
EIS	Electrochemical impedance spectroscopy
FCEV	Fuel cell electric vehicles
HER	Hydrogen evolution reaction
LSV	Linear sweep voltammetry
NF	Ni foam
PVDF	Polyvinylidene fluoride

PEC	Photoelectrochemical
RHE	Reversible hydrogen electrode
TMD	Transition metal halides

Nomenclatures:

H_2	Hydrogen gas

1. Introduction

The ongoing and forthcoming energy crisis and the imminent threat arising from the issue of climate change needs the world to rely on alternative sources of sustainable and clean energy. The efficient and cleaner production of hydrogen (H_2) through electrocatalytic processes, such as the photoelectrochemical division of water or electrolysis coupled with renewable energy sources offers a promising and attractive next-generation energy conversion technique [1–4]. In fuel cell technology, hydrogen is at the heart of energy and environmental problems because it is a clean fuel for various energy conversion devices [5-7] and this makes electrocatalysts extremely important. Currently, fossil fuels and natural gases are the main source for the production of H_2 but it generates carbon emissions. Due to all these drawbacks, researchers are working on finding ways to generate hydrogen using renewable technologies such as water splitting. To achieve water splitting, the hydrogen evolution reaction (HER) is a crucial mechanism and electrocatalysts are materials necessarily to accomplish HER. Consequently, HER during electrochemical splitting of water has been the focus of many researchers around the world (Fig. 1). Splitting water into hydrogen and oxygen is one of the most interesting and cheapest options for conserving renewable energy [11-14].

As an ideal renewable energy, hydrogen based focus has attracted a lot of attention because of its high energy density and environmental benignity [15]. It is well documented that platinum group metals (PGM) are the most efficient electrocatalysts for HER ($2H^{++} 2e^- = H_2$) [24,25]. Metallic platinum (Pt) shows a favourable activity for HER in acidic and alkaline media [16], however, the high cost and limited availability of Pt requires alternative and inexpensive catalysts [17-19]. In this context, it is of utmost importance to develop inexpensive and high efficiency HER electrocatalysts for Pt replacement and this review is dedicated to summarise great efforts that are made in developing highly active and resistant HER without Pt for economic production of hydrogen.

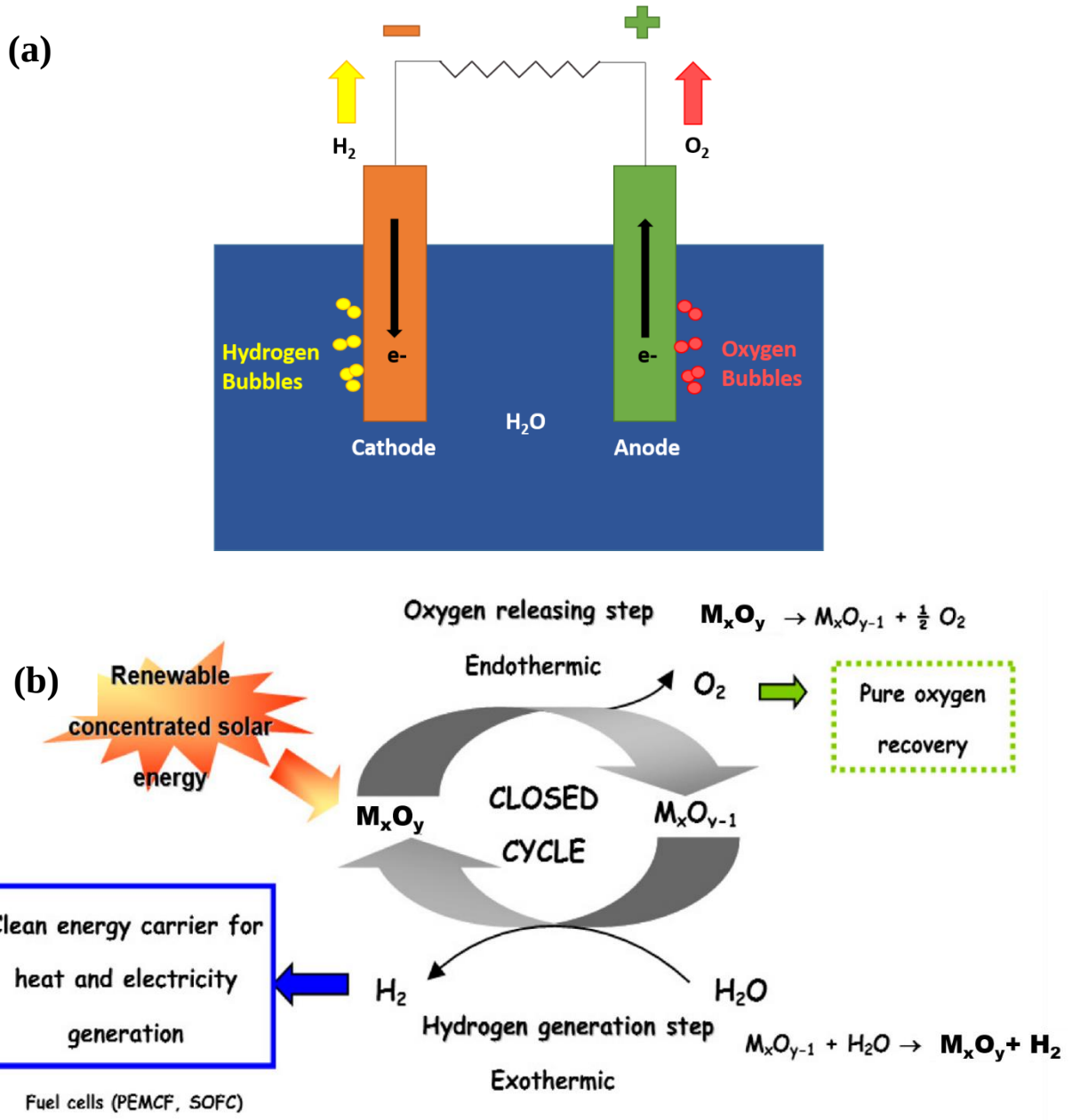

Fig. 1 (a) Water splitting mechanism (b) Strategies to generate hydrogen using transition metal [15]

HER mechanisms

Two mechanisms are commonly understood to describe the HER (i) the Volmer–Tafel and (ii) Volmer– Heyrovsky mechanisms [1]. In acidic solutions (Equations (1)–(3) where * denotes a free site on the surface and H^* denotes a hydrogen atom adsorbed on the surface), the adsorbed hydrated protons (H_3O^+) are reduced to produce H^* (intermediate) via a Volmer step; subsequently, two H^*

combine to form one H_2 molecule via a Tafel route or one H^* reacts with the hydrated proton to form hydrogen through a Heyrovsky step.

$H_3O^+ + e^- \rightarrow H^* + H_2O$ (Volmer step)……...(1)

$H^* + H^* \rightarrow H_2$ (Tafel step)……...(2)

$H^* + H_3O^+ + e^- \rightarrow H_2 + H_2O$ (Heyrovsky step)…….....(3)

In comparison, Equations (4)–(6) shows the HER mechanism in neutral and alkaline electrolytes. In detail, H^* is generated from the reduction of water molecules, followed by either a combination of 2 H^* (a Tafel step) or the reaction between H^* and H_2O (a Heyrovsky step) to produce H_2.

$H_2O + e^- \rightarrow H^* + OH^-$ (Volmer step)……...(4)

$H^* + H^* \rightarrow H_2$ (Tafel step)……..(5)

$H^* + H_2O + e^- \rightarrow H_2 + OH^-$ (Heyrovsky step)……..…(6)

In both mechanisms, HER is a two-step reaction, where either the Volmer step (adsorption) or the Heyrovsky/Tafel step (desorption) determines the reaction rate. Particularly, the pH of the electrolytes exerts a profound influence on the mechanism. In acidic solutions, the adsorption and electrochemical conversion of protons dominate the reaction kinetics in the Volmer step; while in neutral or alkaline conditions, the H_2O dissociation and OH^- desorption also play a crucial role in determining the rate kinetics. Besides, a Tafel slope is strongly related to reaction kinetics and acts as an indicator of the rate-determining step. In particular, the Volmer, Heyrovsky and tafel steps are reflected from the Tafel slope of 120, 40 and 30 $mV \cdot dec^{-1}$. Interestingly, under a high hydrogen coverage over 0.6, 120 $mV \cdot dec^{-1}$, the Tafel slope is also seen for the Heyrovsky step, suggesting the potential and coverage dependence of tafel slope [20].

Various types of transition metals (Co, Fe, Ni, W and Mo) have been selected as effective electrocatalyst for HER in recent years as well as their derivative components. Various types of abundant transition metal compounds on earth such as MoS_2, WS_2, amorphous MoS_x, CoS_2, $CoSe_2$, CoP, Ni_2P, FeP, MoP, MoP and Ni-Mo alloy have recently been identified as promising HER electrocatalysts In this review, cheap and effective transition metals, such as molybdenum (Mo) & tungsten (W) were brought forward to be highlighted due to their high similarity with the

metals of the Pt group and their promising potentials as cost-effective electrocatalysts for HER [21, 22]. Mo, W, Pt, these all are d-block 2D transition metals. However, these single metal atom electrocatalysts are prone to aggregation, due to the large surface energy of the single metal atoms, even though they are good electrocatalysts for HER with low overpotentials. Among all these platinum (Pt) and Pt-group noble metals are rare and expensive, thus leading to the limitation of their applications in large scale, while Mo and W are alternative cost-effective electrocatalysts for the platinum-based systems. The intrinsic properties of transition metals include hydrogen adsorption Gibbs free energy ΔG_H, active sites and electronic conductivity, which plays a fundamental role in determining the catalytic activity of HER. As a good activity descriptor, it is found that ΔG_H largely determines the overall reaction kinetics of the HER. The ΔG_H is always acquired through theoretical calculations, while the exchange current density can be obtained by experimental measurement. if the adsorption of hydrogen is too weak ($\Delta G_H > 0$), it is difficulty for the combination of the proton and electrocatalyst, thus leading to a limited Volmer step. In turn, if the adsorption is too strong ($\Delta G_H < 0$), the adsorbed hydrogen is hard to separate from surface of electrocatalysts, resulting in a limited desorption process (via either a Heyrovsky step or Tafel step) due to the active sites mostly occupied. That means the value of ΔG_H closer to zero indicates the higher catalytic activities. Pt with a hydrogen adsorption Gibbs free energy (ΔG_H) of 0.09 eV, whether it is 0.08 eV for Mo and 0.07eV for W, which both approach 0 eV, indicates a remarkable enhancement [18,19].

2. Mo-based electrocatalysts for HER

2.1 Evaluation of the performance of electrocatalysts based on nanostructures of molybdenum for the HER

The hydrogen generation or evolution using Mo transition metal halides (TMD) has gained interest due to its predominant conductivity, abundancy and low cost. However, there are almost no direct comparisons between the transition metal chalcogenides for LEI. Bhat et al. [22], presented the research study on a series of MoX_2 (X = Se, S, Te) molybdenum chalcogenide nanostructures as an electrocatalyst for HER, $MoSe_2$ nanoflowers, MoS_2 nanograns and $MoTe_2$ nanotubes and reported current densities of 10mA cm^2 in the potential of 208mV, 173mV and 283 mV with measured Tafel slope values of 65.92 mV dec^{-1}, 109.81 mV dec^{-1} and102.06 mV dec^{-1} respectively. In this study, different Mo based electrocatalysts will be briefly introduced by category as follows:

2.1.1 Carbon/Mo based composites

Coupling with a carbon matrix or additives can increase surface area improving Mo dispersion and control particle size due to a mesoporous structures, nanoscale morphology and protective shell [20, 24-29]. In addition, integration with conductive carbons e.g., graphene, carbon nanotubes, and carbon black facilitates charge transport and accelerates reaction kinetics [30-33] that are discussed in this section.

As reported by Gao et al. [20], various carbon materials including nanotubes [77], nanosheets [34], quantum dots [35] and nanofibers [36] with nanostructures can be introduced to Mo based catalysts to increase the surface area which enhances electron transfer. For example, by carbonizing the Mo–melamine polymer precursor on carbon nanotubes (CNTs), a high dispersion of β-Mo_2C nanoparticles and enhanced electric conductivity were both realised, delivering a much lower onset potential vs reversible hydrogen electrode (RHE) (−195 mV for 10 $mA \cdot cm^{-2}$) than the counterpart without CNTs (−340 mV for same current density), suggesting superior electrochemical activity [29]. Moreover, in this study, a smaller Tafel slope of 75 $mV \cdot dec^{-1}$ was obtained for Mo_2C/CNT than the 110 $mV \cdot dec^{-1}$ for the control sample, indicating a lower activation energy and faster reaction kinetics. The outstanding HER performance could be attributed to the abundant active sites on the uniformly dispersed Mo_2C for H adsorption and activation, and the facilitated charge transport through the Mo_2C–CNT interfaces [37]. Owing to its merits, no decay was observed even after 1000 cycles of cyclic voltammograms, demonstrating its great potential as a highly durable HER catalyst in practical applications. To further immobilize the Mo_2C particles on the CNTs upon thermal treatment, oxalic acid was added to replace the ethoxy by forming oxalate groups with Mo ions (Fig. 2a). Benefiting from the steric hindrance of the complex and interaction with CNTs, the Mo_2C agglomeration was considerably inhibited during the 800 ºC calcination, achieving a highly dispersed nanoparticles of diameter 4 to 8 nm (Fig. 2b) [38].

Also, due to the reduced internal charge transfer resistance, the improved dispersion of active sites and large electrochemical surface area, the Mo_2C/CNTs composite catalyst showed an overpotential of 110 mV over 10 $mA \cdot cm^{-2}$ and stable activity over 15 h and 1000 potentiodynamic sweeps. Additionally, the low Tafel slope of 51.34 $mV \cdot dec^{-1}$ suggested a Volmer–Heyrovsky mechanism, where the Heyrovsky desorption step determined the reaction kinetics [39]. Apart from the promotional effect on active site exposure by enhancing the dispersion and electric

conductivity by increasing the Fermi level, the addition of CNTs exerted a profound influence on the Mo valance state. In particular, more Mo^{3+} were reduced to Mo^{2+}causing a reduced ratio of Mo^{3+}/Mo^{2+} in presence of CNTs, which strengthened the Mo–H bond, accelerating the H_3O^+ reduction in the Volmer step and facilitated the H* adsorption [40] (Fig. 2a).

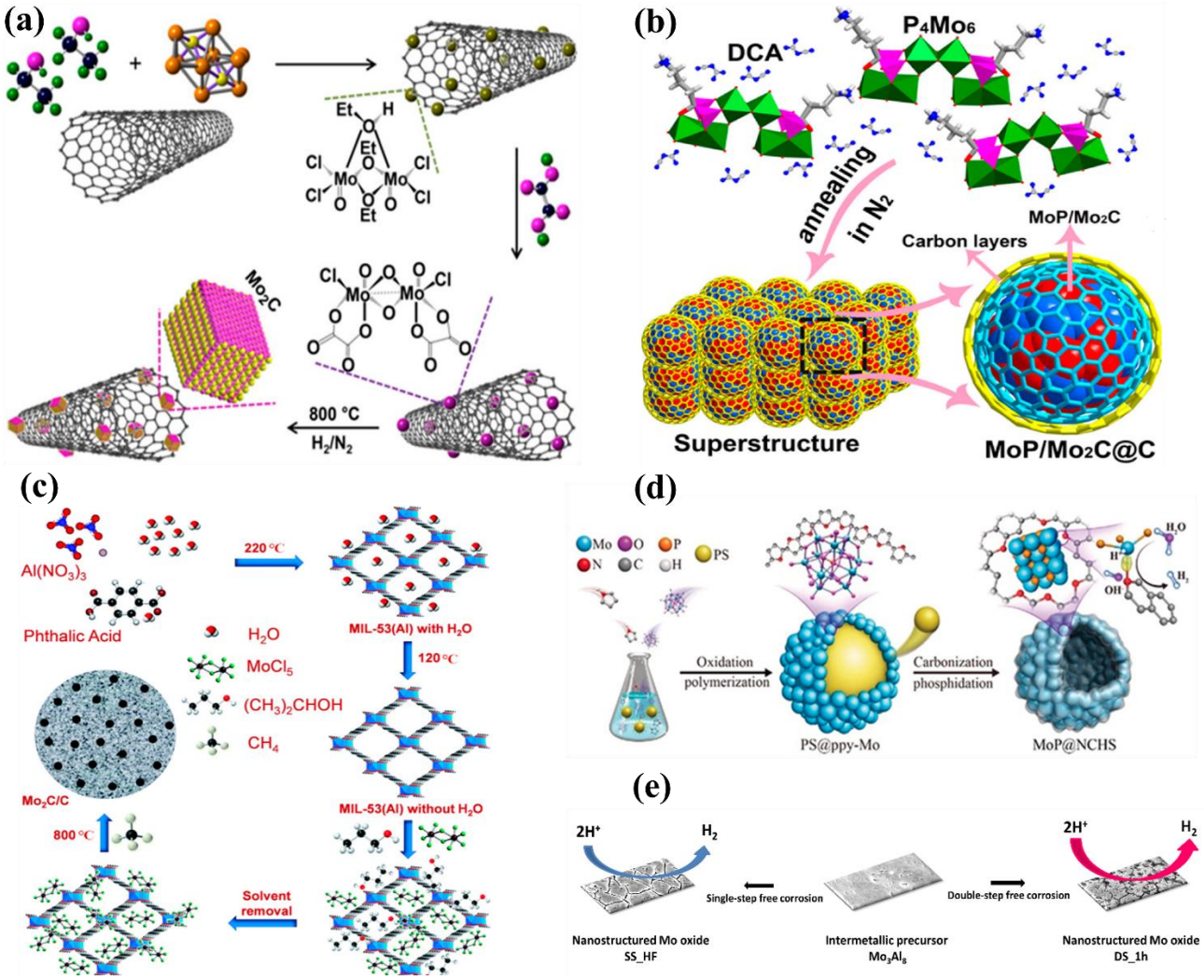

Fig. 2 (a) Growth mechanism of Mo_2C on CNTs surface (b) Preparation schematic of MoP/Mo_2C@C electrocatalyst (c) Formation scheme of Mo_2C/C electrocatalyst (d) Fabrication of MoP/NCHS electrocatalyst [20] (e) Nanostructured molybdenum oxides from aluminium-based intermetallic compounds in HER [21].

To protect Mo species from agglomeration, oxidation and corrosion (etching), a core shell structure was developed with carbon layers as the shell covering the Mo based compounds [25,41, 42]. Meanwhile, the presence of the carbon shell promotes charge transfer through the electrode–electrolyte interfaces [43]. For example, when Mo_2C particles were embedded in the 3D carbon

network and encapsulated by the carbon shell, they interacted intimately with the carbon matrix and were separated from direct contact with the electrolytes, thus facilitating electron transfer and inhibiting corrosion [25]. Moreover, the size of the Mo_2C was only 2 to2.5 nm due to the confinement effect of the carbon shell, possessing a large amount of active sites exposed to the reactant. Thus, in acidic and alkaline electrolytes, lower overpotential of 117 and 121 mV were needed to obtain 10 $mA \cdot cm^{-2}$ current density. In addition, the small Tafel slope of 73.5 $mV \cdot dec^{-1}$ indicated a fast kinetics in HER, benefiting from the high electrochemical active area based on capacitance [44] and low internal charge transfer resistance (Fig. 2b). Different N configurations were compared regarding their contributions to the HER activity of N doped MoP@carbon, including pyrrolic N, pyridinic N and graphitic N [68]. In the preparation, N atoms were introduced by oxidative polymerization of pyrrole initiated by $H_3PMo_{12}O_{40} \cdot nH_2O$ (an Mo precursor). After calcination and phosphidation with the help of polystyrene spheres as the sacrificial template, MoP nanoparticles were encapsulated within the hollow N doped carbon spheres (Fig. 2d). After peak fitting, the N 1s spectra were deconvolved into four configurations (pyridinic N at 397.8 eV, pyrrolic N at 400.5 eV, graphitic N at 401.4 eV and pyridinic N–O at 402.5 eV) [20]. Similarly, in one more research on HER [21], Mo_3Al_8, an intermetallic compound was used as a precursor to obtain nanostructured molybdenum oxides. It was prepared into ribbons by arc-melting and melt-spinning techniques. Single and double-step free corrosion of the as-quenched material was studied in 1 M KOH, 1 M HF and 1.25 M $FeCl_3$ at room temperature. In both cases, a few microns thick nanostructured molybdenum oxides were obtained on the surface layer. Two of the as-prepared samples were tested for their electrocatalytic capability for HER in 0.5 M H_2SO_4 giving low onset potential (−50 mV, −45 mV), small Tafel slopes (92 mV dec^{-1}, 9 mV dec^{-1}) and high exchange current densities (0.08 mA cm^{-2}, 0.35 mA cm^{-2} respectively). They found the proposed nanostructured molybdenum oxides to be cost-effective and sustainable due to the cheap and abundant starting material used and the simple synthetic route, paving the way for their use as HER electrocatalysts (Fig. 2e).

In addition to the preparation of mesoporous carbons from natural products and textiles, metal–organic frameworks (MOFs), as a precursor, can offer a confined environment with abundant pores generated by organic ligands. In particular, an Al-MOF (MIL53) was hydrothermally synthesised which was observed to possess a microporous structure based on the type I curves of adsorption/desorption [20]. Benefiting from the large surface area (1165 $m^2 \cdot g^{-1}$),

$MoCl_5$ was homogeneously impregnated in the MOF frameworks. During the carbonization, Mo2C was in-situ formed from the reduction of Mo species under CH_4 decomposition (Fig. 2c)

2.1.2. Improvements in electrocatalysts stability

Various metals (e.g., Ni, Co) can be doped with Mo based catalysts to improve their HER activity and stability by modulating the electronic structure, enhancing conductivity, tuning the binding energy of *H* and by generating more active sites [45-47]. For example, Hu et al. [27] doped Ni into an Mo_2C/carbon fiber paper hybrid and found that the resistance to charge transfer decreased from 12.7 to 9 Ω compared with an undoped counterpart. More importantly, a good balance was struck between the adsorption and desorption of *H* on/from the Mo_2C by changing the valence state of Mo [48]. Thus, a low overpotential of 121.4 mV at 10 $mA \cdot cm^{-2}$ was exhibited with a 10-h stable operation [28]. To promote the electronic interaction between Ni and Mo, Ni was first electrodeposited on carbon cloth (CC) followed by preparing the Ni–Mo precursor by the hydrothermal treatment of molybdate; after calcination, an Ni-MoO_2/CC hybrid catalyst was formed [49]. Based on the positive shift to 855.8 eV (Ni-MoO_2) from 854.7 eV (Ni) in a Ni 2p XPS spectra, a strengthened interaction was suggested by the electron transfer from Ni to Mo [49]. Due to the strong Ni–Mo interaction, the O 2p orbitals in MoO_2 were upraised, thus facilitating the hydrogen adsorption [51, 52]. In the meantime, water adsorption and dissociation got improved on the positive charged Ni species, further enhancing the *H* adsorption on MoO_2. The modified metal–H bonds could interact with H_2O molecules and electrons to release H_2 via the Heyrovsky step (neutral and alkaline electrolytes) and Tafel recombination step (acidic electrolyte) [53]. As a result, this robust HER catalyst presented a low overpotential of 84, 69 and 46 mV at 10 $mA \cdot cm^{-2}$ in neutral, acidic and alkaline electrolytes with a superior stability over 36 h in all pH ranges [49].

Apart from Ni doping, the dual atoms doping of Ni and Co synergistically optimizes the metal–H binding energy and facilitates electron transport. Through a facile physical mixing and calcination, Co, Ni codoped MoO_2 possessed a homogeneous dispersion of Co, Ni, Mo and O elements. The weak Co–H and Ni–H bonds modulated the hydrogen adsorption and desorption behaviors. In addition, a larger electrochemical active area was enabled for co-doped MoO_2, based on the higher C_{dl} value of 7.7 $mF \cdot cm^{-2}$, than the single doping (5.5 and 5.6 $mF \cdot cm^{-2}$ for Co- and Ni-MoO_2, respectively). Moreover, benefiting from the optimized electronic structure, charge transfer

resistance was reduced with the dual doping, favoring a fast HER kinetics [54, 55]. As a consequence, the overpotential to achieve 10 $mA \cdot cm^{-2}$ was smaller for Co, Ni co-doped MoO_2 (103 mV) in comparison to Co-MoO_2 and Ni-MoO_2. Table 1 shows a summary of the representative Mo based electrocatalysts for hydrogen evolution reaction gathered from the literature.

Table 1: Summary of Mo based electrocatalysts for HER

Catalyst	Electrolyte	Overpotential at 10 $mA \cdot cm^{-2}$ (η_{10})	Tafel Slope/($mV \cdot dec^{-1}$)	Ref
NP-Mo_2C	0.5 M H_2SO_4	210	64	24
Mo_2C/C	0.5 M H_2SO_4	117	60.5	25
	1 M KOH	121	73.5	
Mo_2C/CNFs	0.5 M H_2SO_4	160	66	26
	1 M KOH	92	63	
MoP/Mo_2C@C	1 M KOH	75	58	35
MoC-MoP/N-CNFs	0.5 M H_2SO_4	158	58	56
	1 M KOH	137	65	
Mo_2C/GNR	0.5 M H_2SO_4	152	65	57
	1 M KOH	121	54	
Mo_2C/N-C	0.5 M H_2SO_4	155	73	58
	1 M KOH	78	64	
Mo_2C/C	1 M KOH	165	63.6	59
Co/Ni-MoO_2	1 M KOH	103	80	60
MoO_2/MoS_2|P	1 M KOH	45	64.2	61
MoO_2-Ni	0.5 M H_2SO_4	69	31	49
	1 M PBS	84	75.3	
	1 M KOH	46	56.9	
MoP@NPSC	0.5 M H_2SO_4	71	75	62
MoP@NCHSs	1 M KOH	92	62	63
	1 M KOH	42	127	64

CoP–MoO_2/MF	0.5 M H_2SO_4	65	85	
MoS_2/MoO_2	1 M KOH	157	119	65

The transition metal carbides/nitrides referred to MXenes also as a wonder material presenting newer opportunities owing to their unique properties such as high thermal and electrical conductivity, high negative zeta-potential and mechanical properties similar to the parent transition metal carbides/nitrides. These properties of MXenes can be utilized in various societal applications including for energy storage and energy conversion such as for hydrogen evolution [56]. Few literatures are reported on MXenes for HER such as; 2H-MoS_2 on Mo_2CT_x MXene nanohybrid for efficient and durable electrocatalytic hydrogen evolution. In this study researcher presented a simple and scalable method to circumvent adventitious oxidation in Mo_2CT_x MXenes via in situ sulfidation to form a Mo_2CT_x/2HMoS_2 nanohybrid. The intimate epitaxial coupling at the Mo_2CTx/2H-MoS_2 nanohybrid interface afforded superior HER activities, requiring only 119 or 182 mV overpotential to yield −10 or −100 mA cm^{-2} $_{geom}$ current densities, respectively. Density functional theory calculations reveal strongest interfacial adhesion which was found within the nanohybrid structure as compared to the physisorbed nanohybrid, while showing the possibility to tune the HER overpotential through manipulating the extent of MXene sulfidation. Critically, the presence of 2H-MoS_2 suppresses further oxidation of the MXene layer, enabling the nanohybrid to sustain industrially relevant current densities of over −450 mA cm^{-2} $_{geom}$ with exceptional durability. Less than 30 mV overpotential degradation was observed after 10 continuous days of electrolysis at a fixed −10 mA cm^{-2} $_{geom}$ current density or 100,000 successive cyclic voltammetry cycles. The exceptional HER durability of the Mo_2CT_x/2H-MoS_2 nanohybrid presented a major step forward to realize practical implementation of MXenes as noble metal free catalysts for broad-based applications in water splitting and energy conversion [57]. One more literature published on two-dimensional molybdenum carbide (MXene) as an efficient electrocatalyst for hydrogen evolution. In this study, researcher did computational screening study of 2D layered M_2XT_x (M = metal; X = (C, N); and T_x = surface functional groups) predicted Mo_2CT_x to be an active catalyst candidate for the HER. Researcher synthesized both Mo_2CT_x and Ti_2CT_x MXenes, and in agreement with their theoretical predictions, Mo_2CT_x was found to exhibit far higher HER activity than Ti_2CT_x. Theory suggested that the basal planes of Mo_2CT_x are catalytically active toward the HER, unlike in the case of widely studied MoS_2, in which only the edge sites of the 2H phase were

active. This work paved the way for the development of novel 2D layered materials that can be applied in a multitude of other clean energy reactions for a sustainable energy future [58]. In this area, another study was carried out on tuning the basal plane functionalization of two-dimensional metal carbides (MXenes) to control hydrogen evolution activity. Previous theoretical and experimental results have shown that some two-dimensional (2D) transition metal carbides (MXenes) can be effective electrocatalysts for the HER, based on the assumption that they are functionalized entirely with oxygen or hydroxyl groups on the basal plane. However, it is known that MXenes can contain other basal plane functionalities, e.g., fluorine, due to the synthesis process, yet the influence of fluorine termination on their HER activity remains unexplored. In this research, author investigated the role and effect of basal plane functionalization (Tx) on the HER activity of 5 different MXenes using a combination of experimental and theoretical approaches. They first studied $Ti_3C_2T_x$ produced by different fluorinecontaining etchants and found that those with higher fluorine coverage on the basal plane exhibited lower HER activity. Further they controllably prepared Mo_2CT_x with very low basal plane fluorine coverage, achieving a geometric current density of -10 mA cm^{-2} at 189 mV overpotential in acid. More importantly, their results indicated that the oxygen groups on the basal planes of Mo_2CT_x are catalytically active toward the HER, unlike in the case of widely studied 2H-phase transition metal dichalcogenides such as MoS_2, in which only the edge sites are active. These results paved the way for the rational design of 2D materials for either the HER, when minimal overpotential is desired, or for energy storage, when maximum voltage window is needed [59].

3. W-based electrocatalysts for HER

Tungsten sulfide (WS_2) and tungsten carbide (W_2C) are proposed to be superior candidates for various electrochemical applications, owing to their plentiful active edge sites and better conductivity. In this section, the integration of W_2C and WS_2 was studied by using a simple chemical reaction to form W_2C/WS_2 hybrid as a proficient electrode for HER.

3.1 W_2C nanoparticles for efficient electrocatalytic evolution of hydrogen

Gong et al. [66] reported that W_2C is potentially more active HER than WC. They developed an improved carburetion method and successfully prepared ultra-small and pure phase W_2C nanoparticles. When evaluated by HER electrocatalysis, W_2C nanoparticles showed an onset

potential of 50 mV, a Tafel slope of 45 $mVdec^{-1}$ and excellent long-term cycle stability, which were far better than all the existing WC-based materials.

In one more literature reported by Hussain et al. [67] a simple chemical reduction route was employed to produce the W_2C nanoparticles. The product powder was kept under the gas mixture of H_2 (80 standard cubic centimeters per minute, sccm), CH_4 50 (sccm), and Ar environment in the tubular furnace at 850 °C for 3 h annealing process. Finally, the W_2C powder was collected after the tube attained room temperature. Further they synthesized W_2C/WS_2 hybrid nanostructure and analyzed it’s HER performance. They used About 1 g of commercial W_2C powder by dispersing it in the ethanol solution (50 mL), stirred at room temperature for 3 h. Then 0.25 g WO_3 was dispersed in ethanol and DI water mixture solution followed by 0.5 g of thiourea dissolved aqueous solution blending with the W_2C solution and stirred. After that, 2 mL of hydrazine solution and 30 mL of liquid ammonia were mixed with one-pot solution and stirred for 5 h at 85 °C. The deposit was parted, cleansed with DI water, and dehydrated in a hot oven, overnight, at 60 °C. The powder was post-annealed in a furnace, at 850 °C, for 3 h, under the CH_4 (50 sccm), H_2 (80 sccm) and Ar atmosphere. Fig. 3 illustrate the synthesis of a hierarchically W_2C/WS_2 hybrid nanostructure.

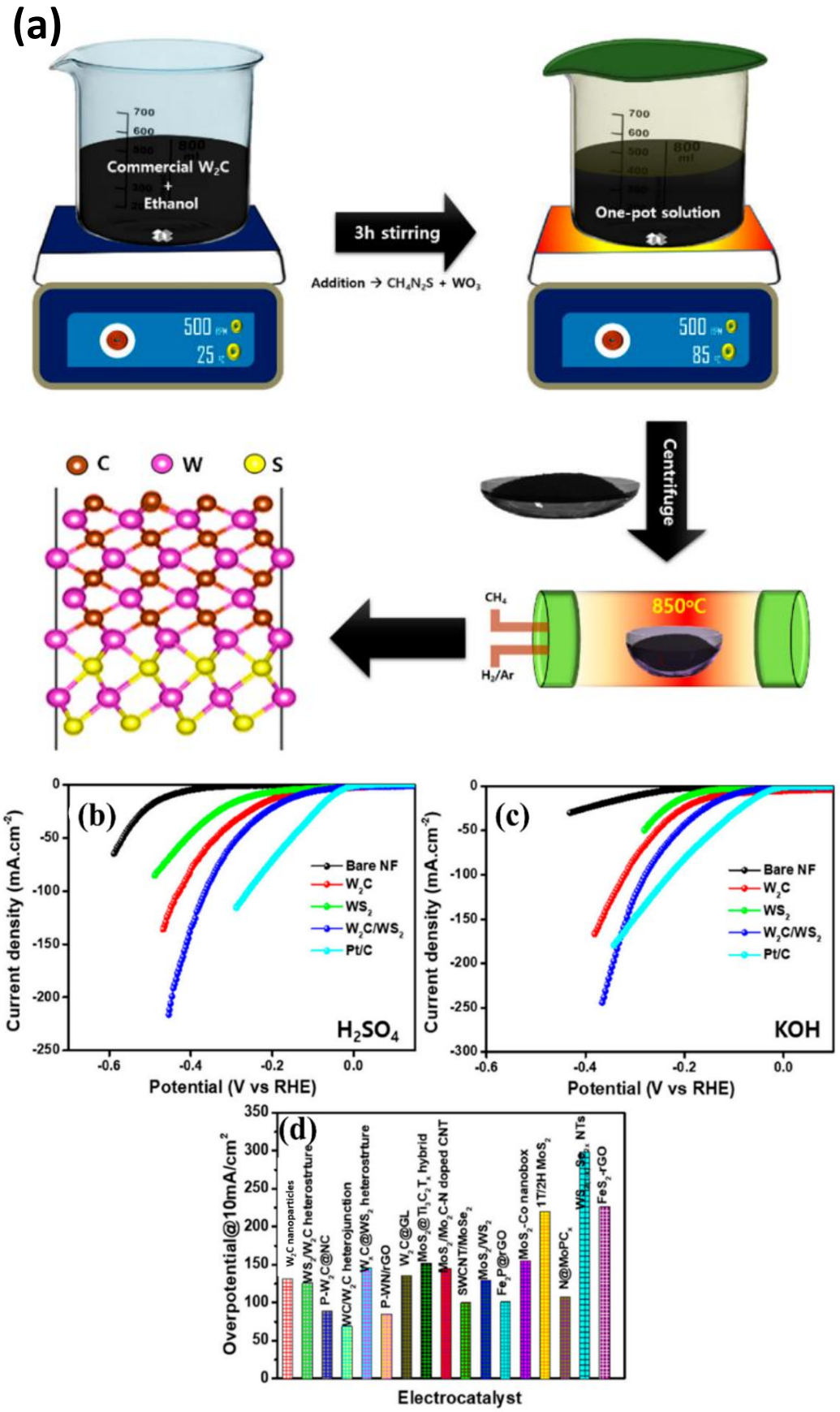
(a)
Commercial W_2C
+
Ethanol
3h stirring
Addition → CH_4N_2S + WO_3
One-pot solution
C
W
S
Centrifuge
CH_4
H_2/Ar
850°C
(b)
Current density (mA.cm^{-2})
Potential (V vs RHE)
Bare NF
W_2C
WS_2
W_2C/WS_2
Pt/C
H_2SO_4
(c)
KOH
(d)
Overpotential@10mA/cm^2
Electrocatalyst
W_2C nanoparticles
WS_2/W_2C heterostrture
P-W_2C@NC
WC/W_2C heterojunction
W_2C@WS_2 heterostrture
P-WN/rGO
W_2C@GL
MoS_2@$Ti_3C_2T_x$ hybrid
MoS_2/Mo_2C-N doped CNT
SWCNT/$MoSe_2$
MoS_2/WS_2
Fe_2P@rGO
MoS_2-Co nanobox
1T/2H MoS_2
N@$MoPC_x$
$WS_{2(1-x)}Se_{2x}$ NTs
FeS_2-rGO

Fig. 3 (a) Synthesis of W_2C/WS_2 hybrid with its derived structure, Hydrogen evolution polarization profiles for Pt/C, bare NF, W_2C, WS_2, and W_2C/WS_2 at 10 mV s^{-1} sweep speed in (**b**) 0.5 M H_2SO_4 and (**c**) 1 M KOH media. (**d**) Overpotential comparison of different electrocatalysts [67]

3.1.1 HER performance

For the working electrode preparation, researchers [67] have used polyvinylidene fluoride (PVDF), active material (W_2C, WS_2, and W_2C/WS_2), and carbon black in 10:80:10 mass ratio and *N*-methyl-2-pyrrolidone (NMP) was added drop-wise. The paste was layered on Ni foam (NF) and dehydrated overnight at 100 °C. For the reference electrode, Ag/AgCl and Hg/HgO were used in acidic and alkaline media performance, respectively, with a graphite counter electrode. They recorded iR corrected linear sweep voltammetry (LSV) by using an electrochemical system (model: 660D; company: CH Instruments, Inc., Austin, TX, USA) in 1 M KOH and 0.5 M H_2SO_4 media, with a scan speed of 10 mV s^{-1}. Electrochemical impedance spectroscopy (EIS) results were noted at the frequencies of 0.01 Hz to100 kHz in acid and alkaline media. The HER potential values were converted for reversible hydrogen electrode (RHE) using the formula E (vs. RHE) = E (vs. Ag/AgCl) + E^0 (Ag/AgCl) + 0.0592 × pH for acidic medium and E (vs. RHE) = E (vs. Hg/HgO) + E^0 (Hg/HgO) + 0.0592 × pH for alkaline medium [67].

3.1.2 Hydrogen evolution studies

Active-materials-coated NFs were engaged as working electrodes to enhance the HER activities in 0.5 M H_2SO_4 and 1 M KOH electrolytes, at room temperature [67]. Fig. 4a shows iR-recompensed LSV polarization profiles in 0.5 M H_2SO_4, using 10 mV s^{-1} sweep speed. The W_2C and WS_2 produced 171 and 242 mV to attain 10 mA cm^{-2}, respectively. In contrast, the W_2C/WS_2 hybrid produced an overpotential of 133 mV at 10 mA cm^{-2} (51 mV @ 10 mA cm^{-2} for Pt/C). The low overpotential shown in this case may be ascribed to the shared interfacial active edges and rapid electron conductivity in the W_2C/WS_2 which proves the importance of hybrid formation. In the 1 M KOH media (Fig. 4b), the W_2C/WS_2 electrode produced highly dynamic HER behavior with a small overpotential of 105 mV at 10 mA cm^{-2} than the WS_2 (189 mV) and W_2C (123 mV). The HER performance of W_2C/WS_2 was superior to most of the hybrid-based electrodes (Fig. 4c) [68-71]. Li et al. [72] prepared the nanocomposite of N, S-decorated porous carbon matrix encapsulated WS_2/W_2C (WS_2/W_2C@NSPC), which delivered the small overpotential of 126 and 205 mV in 0.5 M H_2SO_4 and 1.0 M KOH, respectively. In addition,

Nguyen et al. [73] reported the 170 mV of onset potential with 55.4 mV dec^{-1} of Tafel slope in 0.5 M H_2SO_4 for $W_2C@WS_2$ nanoflowers which were synthesized using the hydrothermal method.

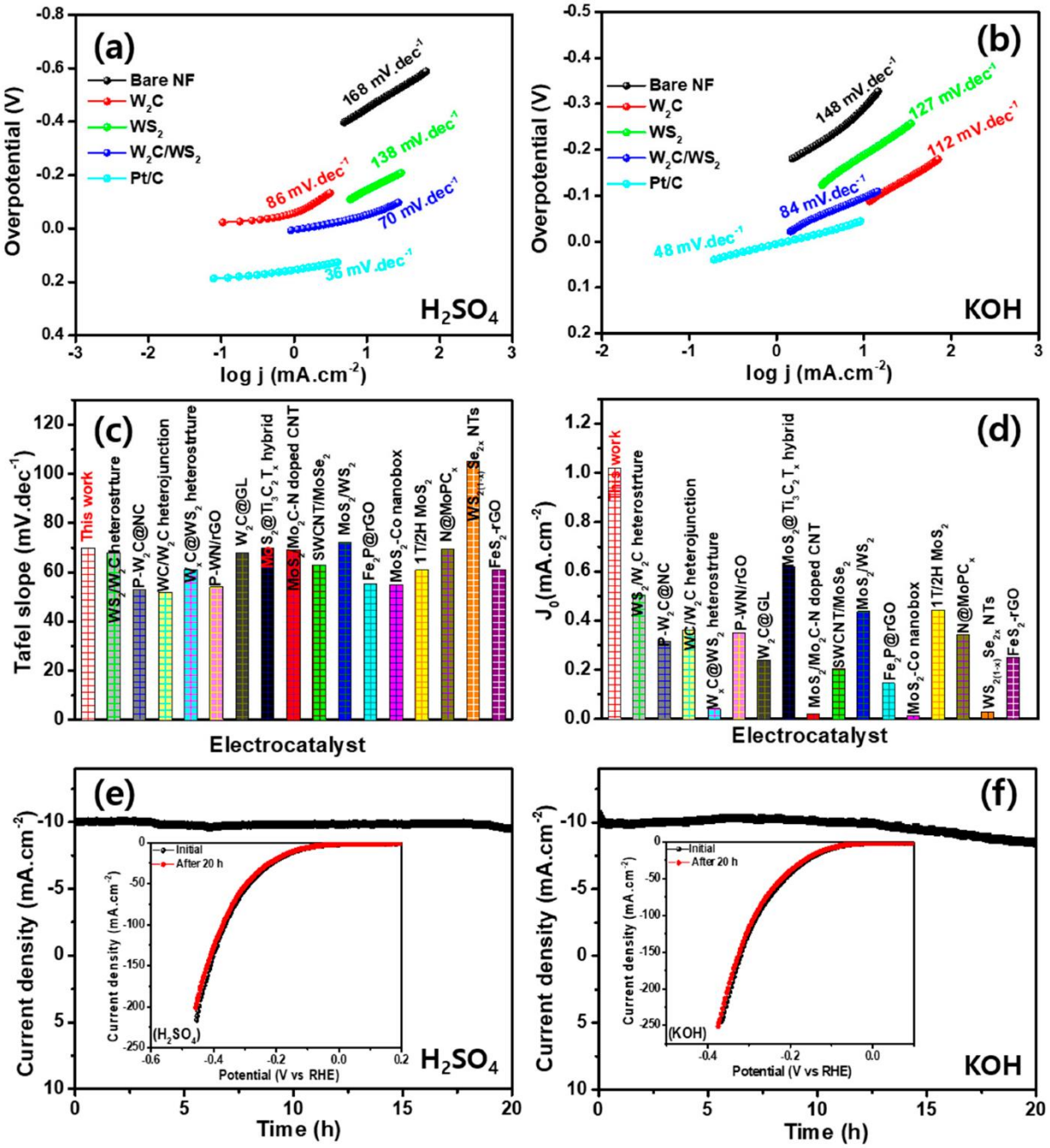

Fig. 4 (a,b) Tafel plots for Pt/C, bare NF, W_2C, WS_2, and W_2C/WS_2 hybrid at 10 mV s^{-1} sweep speed in (**a**) 0.5 M H_2SO_4 and (**b**) 1 M KOH media; comparison of (**c**) Tafel slope and (**d**) exchange current density with different electrocatalysts; chronoamperometric profile of W_2C/WS_2 hybrid for 20 h continuous hydrogen evolution reaction (HER) operation in (**e**) 0.5 M H_2SO_4 and (**f**) 1 M KOH electrolyte (inset: LSV curves before and after 20 h operation) [67]

Tafel slope is a factor which indicates the inherent electrocatalytic activity of the electrode. The Tafel slope values of Pt/C, bare NF, W_2C, WS_2, and W_2C/WS_2 electrocatalysts in H_2SO_4 medium are 36, 168, 86, 138, and 70 mV dec^{-1}, respectively. These values prove the outstanding electrocatalytic activity of the W_2C/WS_2 hybrid. Exchange current densities (j_0) assessed by extrapolation Tafel lines to X-axis and their values observed were about ~1.03, 1.02, 0.55, and 0.19 mA cm^{-2} for Pt/C, W_2C/WS_2, WS_2, and W_2C, respectively. W_2C, WS_2, and W_2C/WS_2 in KOH medium shows Tafel slopes of 141, 127, and 84 mV dec^{-1}, respectively. The small Tafel slope of W_2C/WS_2 also supports high HER behavior of hybrid electrode in the KOH electrolyte. The extrapolated j_0 in KOH electrolyte is 0.93, 0.72, and 0.38 mA cm^{-2} for W_2C, WS_2, and W_2C/WS_2, respectively. The Tafel slope range suggested that HER involved a Volmer–Heyrovsky mechanism for W_2C/WS_2 hybrid, with electrochemical desorption as the rate-regulatory direction [74-77]. Outstanding HER activity in the W_2C/WS_2 hybrid could be explained with electrode kinetics by the accumulated electrocatalytic edge facets and a high ratio of charge transfer. The j_0 and Tafel values are superior to most reported hybrid electrocatalysts (Fig. 4 c,d). The low overpotential, large j_0 value and small Tafel slope in the W_2C/WS_2 hybrid also confirm the importance of hybrid formation for efficient HER electrocatalytic activity in KOH and H_2SO_4 mediums [77-79]. CV profiles were acquired in the non-Faradaic region, to estimate the double-layer capacitance (C_{dl}). The C_{dl} by linear fitting was 3.81 mF cm^{-2} (in H_2SO_4) and 3.33 mF cm^{-2} (in KOH) for the W_2C/WS_2 hybrid. Electrochemical surface areas in H_2SO_4 and KOH were 108 and 83 cm^2 , respectively. A stability and durability evaluation of W_2C/WS_2 electrode was carried out by using chronoamperometric response at a persistent 133 and 105 mV overpotential in H_2SO_4 and KOH (Fig. 4 e,f), respectively. No significant decline was observed over 20 h in the H_2SO_4 medium, whereas slight deterioration was observed in the KOH medium. Researchers noted excellent robustness of W_2C/WS_2 electrode for HER in H_2SO_4, rather than KOH. LSV curves at initial and after 20 h of continuous HER operation are shown in the inset of Fig. 4 e,f, respectively. The summary of observed HER parameters are provided in table 2 for all the measured electrodes.

Table 2. A survey of HER yields of W based electrocatalysts for HER

Materials	Catalyst loading (mg cm^{-2})	Electrolyte	η @ j = 10 mA cm^{-2} (mV)	Tafel slope (mV dec^{-1})	Reference
W_2C/MWNT	0.556	0.5 M H2SO4	123	45	66
WC NPs	1	0.5 M H2SO4	125	84	80
α-WC/CB	0.724	0.5 M H2SO4	260	N/A	81
Thin film W2C	N/A	0.5 M H2SO4	>300	69	82
Thin film WC				91	82
W_2C microspheres	N/A	1 M H2SO4	~170	118	83

4. Hydrogen evolution on reduced graphene oxide-supported PdAu nanoparticles

Lazar et al. [88] reported HER investigation of reduced graphene oxide (rGO)-supported Au and PdAu nanoparticles in an acid solution. Platinum group metals (PGM) are most extensively exploited catalysts for hydrogen evolution reaction (HER). Although PGM-based catalysts are expensive and scarce, they are still widely used for hydrogen production, but for practical use their design aims to limit their amount. Therefore, the synthesis of cost-effective PGM-based catalysts goes in the direction of their minimum consumption by using bimetallic nanoparticles supported by a conductive and cheap material. So, considering all these aspects researchers have investigated hydrogen evolution on Au/rGO and PdAu/rGO electrodes which have shown good performance.

Fig. 5 shows LSV curves and the corresponding Tafel slopes for HER on bare rGO/GC, Au/rGO, and PdAu/rGO electrodes. Beside polarization curves of HER for other materials Fig. 5 a, also presents those for PdAu/rGO recorded after holding the potential at −0.11 V for 10 min, and additionally at −0.04 V for 3 h. The onset potential of approx. −0.25 V for HER on rGO/GC was much higher than for similar carbon-based electrodes [85, 86], including various graphene

structures [86-89]. Besides, higher current densities for a given potential indicate higher activity for HER of the bare rGO/GC substrate electrode used in the work. The onset potential of –0.09 V for HER on Au/rGO obtained by a spontaneous deposition of Au on rGO/GC was the same for Au/GC prepared by the electrochemical deposition of Au on bare GC [91], demonstrating similar catalytic activity of both electrodes.

On the other hand, the PdAu/rGO electrode showed an onset potential of approx. −0.01 V, which is almost equal to the equilibrium potential for HER. This demonstrated the extraordinarily high activity for HER of the electrode consisting of a low atomic percentage of Au and Pd [84, 88]. The PdAu/rGO electrode becomes even more active after holding the potential during the chronoamperometry measurements with the same onset potentials but higher current densities. Comparing the activity of HER for the Au/rGO at the same current density of −5.0 mA/cm^2, the potential for HER shifted positively by 240 mV (from −0.33 V for Au/rGO to −0.09 V for PdAu/rGO), and an additional 30 mV after CA measurements.

Fig. 5b shows the corresponding tafel slopes of HER on the bare and modified rGO electrodes. The high value of −270 mV/dec for bare rGO indicates a slow reaction rate, as already reported in the literature [88-90]. The Tafel slope of −130 mV/dec, obtained for Au/rGO, indicated that the Volmer step is the rate-determining step in the Volmer–Heyrovsky mechanism. The slope was reported for various gold structures [92, 93]. The slope of −65 mV/dec for the PdAu/rGO electrode indicates a faster reaction rate, and a Volmer–Heyrovsky mechanism with a slow Volmer step. The same is obtained in previous works for Pd and Au nanoparticles deposited on a GC substrate [90]. The lowest slope of −46 mV/dec was obtained on PdAu/rGO after CA measurements, which indicated faster kinetics. The same value was obtained for AuPd nanoclusters supported on graphitic carbon nitride [94]. The decrease in the Tafel slope followed the sequence of rGO/GC > Au/rGO > PdAu/rGO > activated PdAu/rGO and it indicated a respective increase in the reaction rate. In addition, the change in the rate-determining step, and the reaction mechanism for all investigated electrodes cannot be determined with certainty due to their dependence on the coverage of adsorbed hydrogen, as well as on the potential as discussed elsewhere [95].

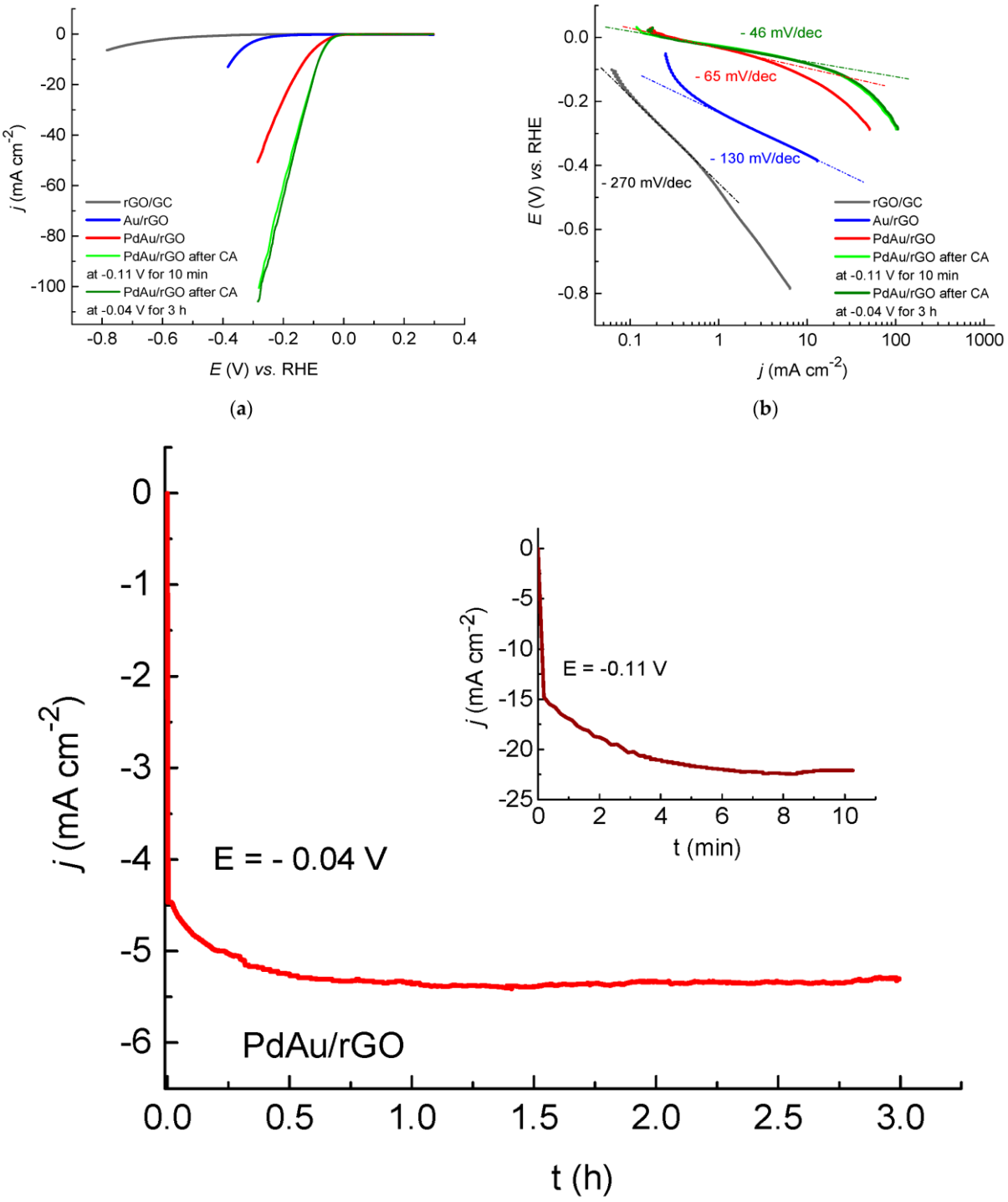

Fig. 5 Hydrogen evolution reaction (HER) on bare rGO, Au/rGO and PdAu/rGO electrodes. (a) LSV curves recorded in 0.5 M H2SO4 at a sweep rate of 10 mV/s and (b) the corresponding Tafel slopes (c) Chronoamperometry measurements recorded on the PdAu/rGO electrode at a constant potential of −0.11 V vs. the reference hydrogen electrode (RHE) for 10 min (insert figure), and at a constant potential of −0.04 V vs. RHE for 3 h [88]

For the stability and durability test, chronoamperometry curves of HER on PdAu/rGO were recorded in deaerated 0.5 M H_2SO_4 at a constant potential and with the electrode rotating at 2500 rpm as presented in Fig. 5c. The PdAu/rGO electrode was first subjected to a potential of −0.11 V for 10 min as shown in Fig. 5c. High hydrogen evolution current densities were immediately reached, with visible bubbles on the electrode surface, achieving a constant value of −22.3 mA/cm^2 after 7 min. The recorded LSV curve showed improved catalytic properties for HER compared to the one before holding the potential (Fig. 5a). In the second CA measurement, the holding potential was –0.04 V, and the duration was 3 h. The activity of HER increased during the first hour then stabilized at −5.3 mA/cm^2. The LSV curve recorded after that showed no difference with the first one recorded after holding the potential for 10 min at −0.11 V (Fig. 5a). These indicated that the PdAu/rGO was activated and stabilized after the first CA measurement. Such activation of the electrode during prolonged test measurements is commonly found in the literature [87, 96, 97].

Besides, the hydrogen yield was calculated from the LSV curves recorded immediately after the PdAu/rGO electrode preparation (red curve in Fig. 5a) and after CA at a constant potential of −0.04 V for 3 h (olive curve in Fig. 5a). Both curves were integrated over the potential range from 0.0 to −0.3 V, i.e., for the hydrogen evolution duration of 30 s. For HER on prepared PdAu/rGO, the amount of evolved hydrogen was 5.2×10^{-10} mol, while after activation during CA measurement, the hydrogen yield was 12.4×10^{-10} mol. Finally, the PdAu/rGO electrode activated during prolonged hydrogen evolution was the most active one concerning both the onset potential and reaction rate. This study revealed a low atomic percentage of both metals on the PdAu/rGO surface, and that PdAu nanoparticles consist of 15% Au and 85% Pd. Besides, the intrinsic Pd activity for HER enhances when diluted with a low amount of Au. Due to the low amount of both metals on the PdAu/rGO electrode, the density and size distribution of PdAu nanoparticles cannot be determined precisely. In many previous studies, the catalytic activity was correlated with the size and composition of PdAu nanoparticles. The catalytic effect of Au addition to Pd for hydrogen production, where it prevents Pd deactivation was also reported for formic acid dehydrogenation over a carbon-supported PdAu catalyst [97]. The effect of the composition on the activity for HER in an acid solution was reported for Pd_xAu_y nanoparticles supported on carbon-based materials [91, 99, 100]. In this case, researchers speculated that graphene edges and other defect sites rich in PdAu nanoparticles provided many active surface sites for proton reduction and subsequent

hydrogen adsorption and evolution. The low content of Au in PdAu nanoparticles contributed to the dilution of the deposited Pd with Au and the formation of more active sites suitable for hydrogen adsorption, not only on the edges but also on top of the PdAu nanoparticles. The activation of the PdAu/rGO electrode for HER is most likely caused by the disintegration and rearrangement of PdAu nanoparticles during HER, either with prolonged cycling (LSV measurements) or while holding the potential in the HER potential region (CA measurements). Such disintegration and rearrangement of the deposited Ru and Os nanoislands spontaneously deposited on Au(111) and induced by higher potentials are previously reported [101, 102], and this most likely occurs during the hydrogen evolution reaction. In this reported study, activity of the PdAu/rGO electrode for the HER was remarkably high, with the overpotential close to zero. HER activity was stable over a 3 h testing time, with a low tafel slope of approx. −46 mV/dec achieved after prolonged hydrogen evolution at a constant potential.

5. RuCo alloy nanoparticles embedded into N-Doped carbon for high efficiency HER

For scalable and sustainable water electrolysis, it is of great significance to develop electrocatalysts that can replace platinum. Currently, it is difficult for most catalysts to combine high activity and stability. To solve this problem, Cheng's research group [103] used cobalt to regulate the electronic structure of ruthenium to achieve high activity, and use carbon matrix to protect alloy nanoparticles to achieve high stability. Herein, based on the zeolitic imidazolate frameworks (ZIFs), a novel hybrid composed of RuCo alloy nano-particles and N-doped carbon was prepared via a facile pyrolysis-displacement-sintering strategy. Due to the unique porous structure and multi-component synergy, the optimal RuCo500@NC750 material in both acidic and alkaline media exhibited eminent HER catalytic activity.

They designed RuCo@NC catalyst for HER. The detailed fabrication process of RuCo@NC is shown in Fig. 6a. Firstly, ZIF67 was synthesized by self-assembly of Co^{2+} and 2-methylimidazole. Subsequently, Ru^{3+} ions were replaced with carbonized ZIF-67 to cover the surface of Co NPs, then sintered to form RuCo alloy NPs loaded on N-doped carbon. These catalysts were called as 1-RuCo-T_2@NC-T_1, 2-RuCo-T_2@NC-T_1, 3-RuCo-T_2@NC-T_1, respectively, according to different Ru content. In addition, Ru NPs/C_{ZIF67}-750 have also been synthesized by $NaBH_4$ reduction for comparison.

The electrocatalytic HER performance of a sequence of samples in acidic (0.5 M H_2SO_4) and alkaline (1.0 M KOH) media was evaluated by researchers [103] using a traditional three-electrode system. For comparison, Ru NPs/C_{ZIF67}-750 and commercial Pt/C (JM, 20 wt.%) were also tested under identical conditions. Firstly, they studied the HER activities of 1-RuCo500@NC-T_1 in alkaline conditions. As shown in Fig. 6b, the LSV curves of 1-RuCo500@NC750 showed the minimum onset potential and maximum current density among the three samples generated at different pyrolysis temperatures, suggesting that 750 °C is the optimal pyrolysis temperature for 1-RuCo500@NC-T_1. The reason may be that there are fewer cobalt nanoparticles produced at 600 °C which finds it difficult to displace Ru and form alloys, while the agglomeration of cobalt nanoparticles at 900 °C leads to the reduction in active sites. Secondly, the HER activities of 1-RuCo-T2@NC750 were tested under alkaline conditions. As shown in Fig. 6c, 1-RuCo500@NC750 has better HER activity than the other two samples. Compared to the pyrolysis temperature, the sintering temperature has less influence on HER activity. Fig. 6d shows that the overpotential of 3-RuCo500@NC750 is very small, only 31 mV at 10 mA cm−2, far lower than the 203.6 mV of Ru NPs/C_{ZIF67}-750 and even the benchmark Pt/C (32.7 mV). At high overpotential, the advantage of 3-RuCo500@NC750 is more obvious (Fig. 6e), indicating that it has good alkaline HER catalytic activity. The Tafel slopes obtained from the polarization curve were utilized to study the intrinsic HER dynamics of catalysts. As shown in Fig. 6f, the Tafel slope (47 mV dec^{-1}) of 3-RuCo500@NC750 was found lower than that of commercial Pt/C (48 mV dec^{-1}) and Ru NPs/C_{ZIF67}-750 (163 mV dec^{-1}), indicating that RuCo@NC-600 has fastest kinetics for HER among them. Furthermore, the low Tafel slope value of 3-RuCo500@NC750 indicated that the HER takes place through the Volmer–Heyrovsky pathway [104]. In alkaline medium, the rate-determining step of both the material and Pt/C is the Volmer step. Since cobalt can accelerate the Volmer step, the material can achieve better performance than Pt/C. Electrochemical impedance spectroscopy (EIS) measurements can further disclose the kinetic characteristics of the catalyst. The charge transfer resistance (R_{ct}) of 3-RuCo500@NC750 is 8.85 Ω, which is much smaller than 24.97 Ω of C_{ZIF67}-750 and 23.04 Ω of Ru NPs/C_{ZIF67}-750, implied that the interfacial charge transfer rate is faster after Ru doping. 3-RuCo500@NC750 showed strong HER activity that it surpassed many of the most advanced catalysts reported to date [103]. Besides, the HER behavior was evaluated by calculating electrochemical surface area (ECSA), which is an important factor in determining overall catalytic activity. Also, the electrochemical double-layer capacitance

(C_{dl}) was linearly proportional to the electrochemical surface area of the catalyst so ECSA was obtained by measuring C_{dl} using cyclic voltammetry (CV) at different scanning rates (0.01~0.1 V s^{-1}).

Researchers reported the C_{dl} value of 3-RuCo500@NC750 is as high as 63.81 mF cm^{-2}, which is the largest among all tested materials. Additionally, it was more than twice that of C_{ZIF67}-750 (30.15 mF cm^{-2}), indicating that the formation of RuCo alloy in the catalyst can offer more active sites to effectively improve HER activity. Durability reflects the long-term stability of the catalyst and is another important index to measure the practical value of electrocatalyst. Firstly, it was evaluated by potential-cycle accelerated durability test (ADT). Through result analysis, 3-RuCo500@NC750 exhibited almost the same polarization curve after 1500 cycles, indicating good durability. Secondly, only a small increase in overpotential was observed in at 15 h chronopotentiometry test, which further proved that it has robust stability in long-term operation. After the accelerated aging test, the crystal phase of 3-RuCo500@NC750 did not change significantly, demonstrated that it had good structural stability in alkaline medium [103, 105-107].

With the development of proton exchange membrane (PEM) electrolysis of water technology, acidic HER has received greater attention [108, 109]. As a consequence, the electrocatalytic HER performance of *n*-RuCo500@NC750 was also investigated under acidic conditions. In 0.5 M H_2SO_4 solution, 3-RuCo500@NC750 requires an overpotential of only 22 mV to obtain the current density of −10 mA cm^{-2}, much lower than that of Ru NPs/C_{ZIF67}-750 (93.2 mV) and slightly higher than that of the reference Pt/C catalyst (15.6 mV). The same is true at high current densities, as shown in Fig. 6 (f, g). Meanwhile, the Tafel slope of 3-RuCo500@NC750 in 0.5 M H_2SO_4 solution was 52 mV dec^{-1}, which is between the reference Pt/C (30 mV Dec^{-1}) and Ru NPs/C_{ZIF67}-750 (90 mV Dec^{-1}), corresponding to a Volmer–Heyrovsky pathway. The low overpotential and Tafel slope indicated that 3-RuCo500@NC750 is an excellent acid electrocatalyst for hydrogen evolution, which exceeds many non-platinum electrocatalysts (Fig. 6i).

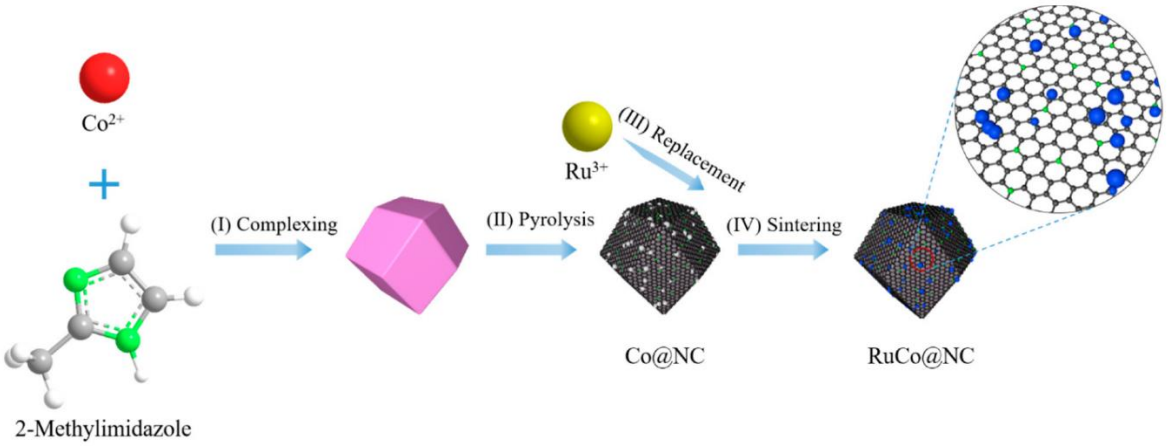
Co2+
Ru3+
(III) Replacement
(I) Complexing
(II) Pyrolysis
(IV) Sintering
2-Methylimidazole
Co@NC
RuCo@NC

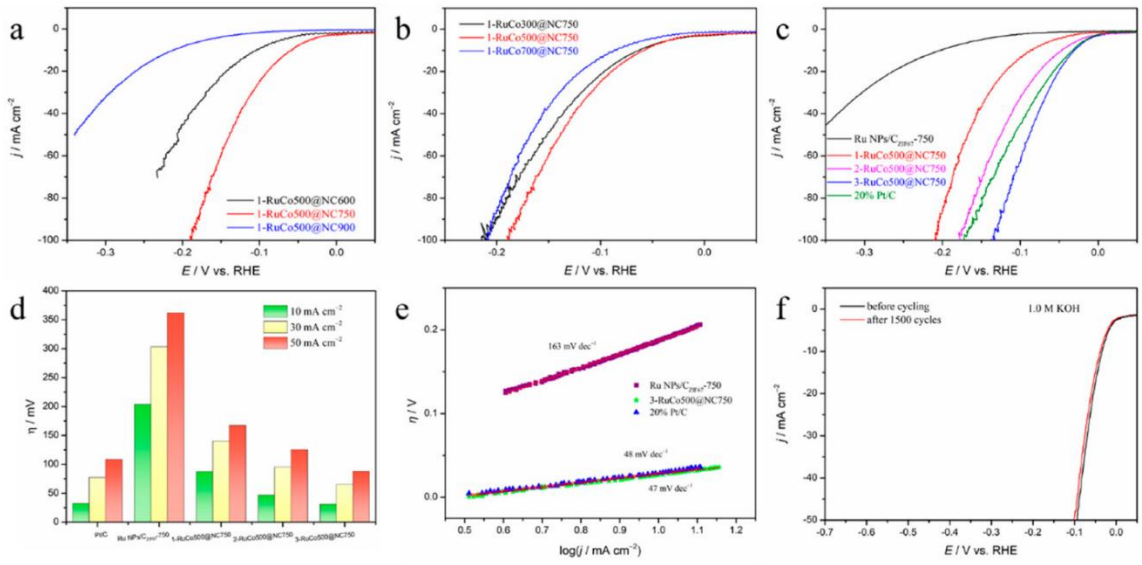
a
b
c
d
e
f
j / mA cm-2
E / V vs. RHE
1-RuCo500@NC600
1-RuCo500@NC750
1-RuCo500@NC900
1-RuCo300@NC750
1-RuCo700@NC750
Ru NPs/C ZIF67-750
2-RuCo500@NC750
3-RuCo500@NC750
20% Pt/C
10 mA cm-2
30 mA cm-2
50 mA cm-2
η / mV
η / V
163 mV dec-1
48 mV dec-1
47 mV dec-1
log(j / mA cm-2)
before cycling
after 1500 cycles
1.0 M KOH

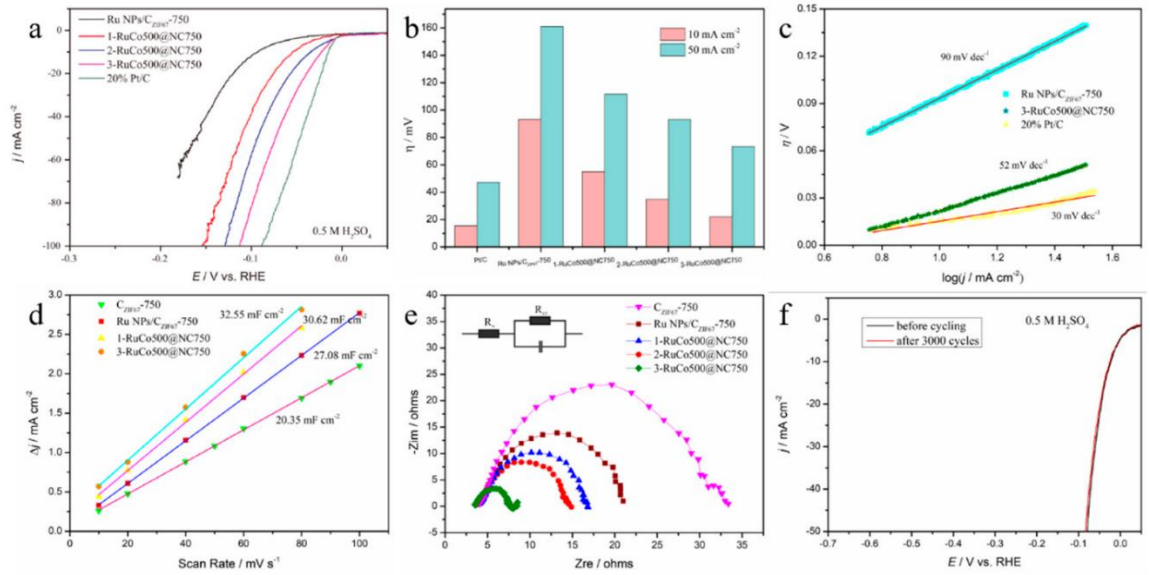
a
b
c
d
e
f
Ru NPs/C ZIF67-750
1-RuCo500@NC750
2-RuCo500@NC750
3-RuCo500@NC750
20% Pt/C
0.5 M H2SO4
E / V vs. RHE
10 mA cm-2
50 mA cm-2
90 mV dec-1
52 mV dec-1
30 mV dec-1
log(j / mA cm-2)
C ZIF67-750
32.55 mF cm-2
30.62 mF cm-2
27.08 mF cm-2
20.35 mF cm-2
Δj / mA cm-2
Scan Rate / mV s-1
-Zim / ohms
Zre / ohms
before cycling
after 3000 cycles

Fig 6. Schematic illustration of synthesis of RuCo@NC by a pyrolysis-displacement-sintering strategy; HER polarization curves of (**a**) 1-RuCo500@NC-T_1 and (**b**) 1-RuCo-T_2@NC750 in 1.0 M KOH. (**c**) Comparison of HER activities of Ru NPs/C_{ZIF67}-750, 20% Pt/C and *n*-RuCo500@NC750. (**d**) HER overpotential of Ru NPs/C_{ZIF67}-750, 20% Pt/C and *n*-RuCo500@NC750 at different current densities (10, 30, 50 mA cm^{-2}). (**e**) Tafel plots of 3-RuCo500@NC750, Ru NPs/C_{ZIF67}-750 and 20% Pt/C catalysts. (**f**) Polarization curves of 3-RuCo500@NC750 initially and after 1500 cycles during the accelerated durability tests. **(g)** HER polarization curves of Ru NPs/C_{ZIF67}-750, *n*-RuCo500@NC750 and 20% Pt/C in 0.5 M H_2SO_4. (**h**) HER overpotential of Ru NPs/C_{ZIF67}-750, 20% Pt/C and *n*-RuCo500@NC750 at different current densities (10, 30, 50 mA cm^{-2}). (**i**) Tafel plots of 3-RuCo500@NC750, Ru NPs/C_{ZIF67}-750 and 20% Pt/C. (j) Linear fitting of capacitance current to CV scan rate for Ru NPs/C_{ZIF67}-750, *n*-RuCo500@NC750 and C_{ZIF67}-750. (**k**) Nyquist plots of Ru NPs/C_{ZIF67}-750, *n*-RuCo500@NC750 and C_{ZIF67}-750. (**l**) Polarization curves of 3-RuCo500@NC750 initially and after 3000 cycles during the accelerated durability tests [103].

Although its hydrogen evolution activity is not as good as that of commercial 20 wt.% Pt/C, its cost is lower, so it still has some practical value for acidic HER. Likewise, the electrochemical double-layer capacitance by cyclic voltammetry was also obtained at different scan rates. The C_{dl} value of 3-RuCo500@NC750 was seen to be the largest among the tested samples (Fig. 6j), indicating that it has the largest ECSA. From the point of view of the electrochemical impedance spectrum (Fig 6k), 3-RuCo500@NC750 has the smallest charge transfer resistance (4.34 Ω), which is beneficial to reduce the energy consumption in the process of hydrogen evolution. In addition, the 3-RuCo500@NC750 also possess the prominent cycling and long-term stabilities in acidic media, as assessed by chronopotentiometric measurements and the electrochemical accelerated durability tests (Fig. 6l). After 3000 scanning cycles, the performance degradation of 3-RuCo500@NC750 was almost negligible. In chronopotentiometry, 3-RuCo500@NC750 maintained high HER activity for up to 15 h. Comparing the XRD patterns of the catalysts before and after the accelerated aging experiment, it was found that the crystal phase structure of the catalysts had little change, indicating that the catalyst had good stability and can run for a long time under acidic conditions.

Based on the foregoing results and discussions [103], the excellent electrocatalytic HER performance of 3-RuCo500@NC750 may be attributed to its unique composite structure and composition, mainly considering that (i) the large electrochemical surface area provides more active sites for catalysis and the three-dimensional porous structure is beneficial for mass transport [110, 111] (ii) Nitrogen-doped graphitized carbon matrix can improve the conductivity of the catalyst, which is conducive to rapid transfer of electrons [112]. At the same time, the carbon matrix can protect the alloy nanoparticles from corrosion and prevent them from agglomeration

[113]. (iii) Alloy effect: According to the *d*-band center theory, the d-band center (E_d) energy level determines the adsorption intensity between the active site on the catalyst surface and the adsorption molecule [114, 115]. The higher the energy level is, the stronger the adsorption capacity [116]. Due to the high E_d energy level of single metal Ru, its adsorption capacity with H is strong, so its activity is poor when used as HER catalyst [117]. Co atoms, which are less electronegative, contribute electrons to Ru atoms when they form alloys. The electrons preferentially enter the bonding orbital of Ru, which reduces the E_d energy level of Ru, thus decreasing the strength of the Ru-H bond [113, 115,117]. In summary, the 3-RuCo500@NC750 catalyst has outstanding catalytic performance due to the advantages of the structure and composition mentioned above. Due to the unique porous structure and multi-component synergy, the optimal RuCo500@NC750 material in both acidic and alkaline media exhibited eminent HER catalytic activity. Notably, the 3-RuCo500@NC750 obtained a current density of 10 mA cm^{-2} at 22 mV and 31 mV in 0.5 M H_2SO_4 and 1.0 M KOH, respectively, comparable to that of the reference Pt/C catalyst. Furthermore, the Tafel slopes of the catalyst are 52 mV Dec^{-1} and 47 mV Dec^{-1}, respectively, under acid and alkali conditions, and the catalyst has good stability, indicating that it could have broad application prospects in practical electrolytic systems. This work analysis reported here to understanding the role of carbon-supported polymetallic alloy in the electrocatalytic hydrogen evolution process, and provides some inspiration for the development of a high efficiency hydrogen evolution catalyst. Other than above compositions for HER, M. Umer et al., reported; out of ~364 catalysts, they found 20 more promising catalysts which exhibited excellent stabilities and superior activities toward the HER. Particularly, Pd@B_4, Ru@N_2C_2, Pd@B_2C_2, Pt@B_2N_2, Ir@h-BN, Fe@C_3, Rh@C_3, and Pd@2DCP and ML-recommended systems Fe@P_3, Mn@P_4 and Fe@P_4 exhibited an ultrasmall magnitude of the HER overpotential (0.01 to 0.03 V), much better than that of commercial Pt based catalysts [120-123].

6. Commercialisation and current market

Fuel cells are a promising technology to be used as a source of heat and electricity for buildings and as a source of electricity for electric motors to drive vehicles. Hydrogen needed for fuel cells can be reformed from methanol, natural gas or even gasoline but these are costly extraction methodologies [114]. Further research efforts are required to develop cost effective and benign environmental friendly technologies through electrolysis process for producing the hydrogen fuel

for clean generation of hydrogen through water splitting thus achieving “net-zero” energy generation methods for reducing our carbon footprint on the environment.

Annually, 98% of the 600 billion cubic meters H_2 globally is produced from natural gas (CO_2 as a byproduct) and only 2% is produced by electrolysis of H_2O. Over 90 % of this (produced from natural gas) is used as a component for fertilizers or consumed in the petrochemical & oil refining industries. Production of hydrogen & distribution infrastructure both are dependent on the government initiatives for investment in this area to setup ambitious projects for achieving ”net-zero” energy targets. At present, the main obstacle in tapping the full potentials of hydrogen technology is the lack of safe infrastructure as a slight leak of H_2 can lead to catastrophic disasters. Few industries working on hydrogen fuel infrastructure are emerging from the automobile sector [124].

Toyota Mirai, the world's most popular FCEV, was launched in the United Arab Emirates in October 2017, when the country's first hydrogen station was opened by local Toyota distributor Al-Futtaim Motors from Masdar City of Abu. Dhabi and Air Liquide of France. Although these projects were pilot studies, these regional projects are supported by the increasingly evident reality of the hydrogen economy in the Asian markets and in particular in Japan, where 100 filling stations have already been established and the government aims to have 800,000 FCEVs on road by 2030 and setting a target of 90% cost reduction of hydrogen by 2050 [125].

8. Conclusion and future directions

In this review, a comprehensive summary of the recent development of Mo based electrocatalysts for the hydrogen evolution reaction (HER) is presented. The fundamentals of HER and representative Mo compounds catalysts are introduced following a series of active initiatives in developing hybrid Mo based structures. Particularly, by coupling with carbon nanostructures, doping with heteroatoms (nonmetallic and metallic elements), and constructing heterostructures, HER activity and stability are both enhanced. The improved performances can be attributed to the modulated adsorption, conversion and desorption of reactants and intermediates, the faster transport of electrons and ions, improved wettability and increased number of active sites. Despite exciting progress, several issues are still needing scientific solution. The review also offers fresh insights into the W-based electrocatalysts for HER, their electrocatalytic and hydrogen evolution.

Next, we discussed about the electro-catalytic activity of some composites such as reduced graphene oxide-supported PdAu nanoparticles and RuCo alloy nanoparticles embedded into n-doped carbon; which have shown excellent electro-catalytic activity for HER.

As we know is already earmarked to be the future fuel in the race to achieve “net-zero” targets in view of the imminent threat of the climate change the world is facing today. While various technologies can be used to generate hydrogen, only a few of them can be considered environmentally benign and friendly. Future efforts for generation of hydrogen may include artificial photosynthesis process through water splitting which could be a promising approach to store solar energy in the form of hydrogen in a scalable way. This is called as the photoelectrochemical (PEC) division of water. In the PEC water division, hydrogen can be produced from water just by using sunlight and specialised semiconductors called photoelectrochemical materials, which would use light energy to directly dissociate water molecules into constituting elements of hydrogen and oxygen. It is still long-term technological path, with the potential for low or zero greenhouse gas emissions. Continuous improvements in efficiency, durability and costs are still needed for market profitability.

Hydrogen production technologies must be improved and expanded through research, development, and experimentation. Efforts to reduce manufacturing costs, maximize productivity, and establish carbon sequestration methods are needed. Improved strategies are required for fundamental hydrogen generation and uniformly distributed hydrogen production. SMR, multifuel gasifiers, water electrolysis, PEC electrolysis, biological technologies, and advanced techniques, such as biomass pyrolysis and nuclear thermochemical water splitting, should emphasize initiatives. On the other hand, global energy projections must accept that they cannot accurately portray future energy systems since they do not include all of the necessary minute elements and complexities. Much more transparency about the techniques and input assumptions underlying energy projections are required so that the consequences of the outcomes may be appropriately comprehended. Simulations designers should also strive to regularly improve their practices, drawing on results from other sources. The impact of emerging innovations in future energy systems may be explored in various ways, including phenomenological possibilities and more comprehensive energy system modeling in lower domains. This exploration should be taken into consideration. Additionally, there are obstacles related to hydrogen storage, distribution, and

transportation that negatively influence the widespread utilization of hydrogen as a transmitter and vector of energy. As a result of its high combustibility and exothermicity, hydrogen storage systems must fulfill strict regulatory standards. Several factors limit the practical utilization of hydrogen in passenger or heavy-duty vehicles, such as hydrogen's high gravimetric and volumetric density. Hydrogen production, distribution, and uses might be commercialized if sophisticated hydrogen synthesis and storage techniques are developed.

Acknowledgments

SG acknowledge the financial support provided by the UKRI via Grants No. EP/S036180/1, EP/T001100/1 and EP/T024607/1, feasibility study awards to LSBU from the UKRI National Interdisciplinary Circular Economy Hub (EP/V029746/1) and Transforming the Foundation Industries: a Network+ (EP/V026402/1) and Hubert Curien Alliance Award from the British Council.

CRediT authorship contribution statement

J. Verma: Conceptualization, Methodology, Investigation, Data curation, writing – original draft, S. Goel: Review, editing & supervision

Declaration of Competing Interest

The author (s) declare that they have no known competing financial interests or personal relationships that could have appeared to influence the work reported in this paper**.**

References:

1. Kano M, Çengel Y-A, Cimbala J-M. Fundamentals and Applications of Renewable Energy. McGraw-Hill Education: New York, NY, USA, 2020.
2. Jin H, Sultan S, et al. Simple and Scalable Mechanochemical Synthesis of Noble Metal Catalysts with Single Atoms toward Highly Efficient Hydrogen Evolution, Adv. Funct. Mater. 2020; 30: 2000531.
3. Tiwari JN, dang NK, et al. Multi-heteroatom-doped carbon from waste-yeast biomass for sustained water splitting, Nat Sustain. 2020; 3: 556–563.

4. Harzandi, A. M. Shadman, S. et al., Immiscible bi-metal single-atoms driven synthesis of electrocatalysts having superb mass-activity and durability. Appl. Catal. B Env. 2020, 270, 118896.
5. Strielkowski W, et al. Renewable Energy in the Sustainable Development of Electrical Power Sector: A Review. Energies, 2021; 14: 1-24.
6. Ucal M, Xydis G. climate changes and sustainable development: Technoeconomic analysis. Sustain. Cities Soc. 2020; 60: 102210.
7. Nasr A-K, et al. Assessment of barriers to renewable energy development using stakeholders approach. Entrep. Sustain. Issues 2020; 7: 2526–2541.
8. Aghahosseini A, Breyer C. Assessment of geological resource potential for compressed air energy storage in global electricity supply. Energy Convers. Manag. 2018; 169: 161–173.
9. Dudin M-N, et al. Study of innovative technologies in the energy industry: Nontraditional and renewable energy sources. Entrep. Sustain. Issues 2019; 6: 1704–1713.
10. Nassar N, Tvaronavi˘ciene M-A. A systematic theoretical review on sustainable management for green competitiveness. Insights Reg. Dev. 2021; 3: 267–281.
11. Brozyna J, et al. Renewable energy and EU 2020 target for energy efficiency in the Czech ˙ Republic and Slovakia. Energies 2020; 13: 965.
12. Sultan S, Tiwari JN, et al., Single Atoms and Clusters Based Nanomaterials for Hydrogen Evolution, Oxygen Evolution Reactions, and Full Water Splitting. Adv Energy Mater 2019; 9: 1900624.
13. European Commission. Renewable Energy Statistics. 2021. Available online: https://ec.europa.eu/eurostat/statistics-explained/ (accessed on 18 October 2021).
14. Tiwari JN, Sultan S, et al., Multicomponent electrocatalyst with ultralow Pt loading and high hydrogen evolution activity. Nat Energy 2018; 3: 773–782.
15. Abanades S. Metal Oxides Applied to Thermochemical Water-Splitting for Hydrogen Production Using Concentrated Solar Energy. ChemEngineering 2019; 3: 1-28.
16. Villafán-Vidales H-I, et al. An overview of the solar thermochemical processes for hydrogen and syngas production: Reactors. Renew. Sustain. Energy Rev. 2017; 75: 894–908.

17. Bhalothia D, et al. H_2 Reduction Annealing Induced Phase Transition and Improvements on Redox Durability of Pt Cluster-Decorated Cu@Pd Electrocatalysts in Oxygen Reduction Reaction. ACS Omega 2019; 4: 971-982.

18. K Zhu, et al. Two-dimensional transition-metal dichalcogenides for electrochemical hydrogen evolution reaction, Flatchem. 2019; 18: 100140.
19. Zhang C, et al. The OH−-driven synthesis of Pt−Ni nanocatalysts with atomic segregation for alkaline hydrogen evolution reaction. J. Mater. Chem. A 2019; 7: 5475−5481.
20. Gao X, et al., Smart Designs of Mo Based Electrocatalysts for Hydrogen Evolution Reaction. Catalysts 2022; 12: 1-25.
21. Raj D, et al. Nanostructured Molybdenum Oxides from Aluminium-Based Intermetallic Compound: Synthesis and Application in Hydrogen Evolution Reaction. Nanomaterials 2021; 11: 1313.
22. Wei Y. Design of efficient electrocatalysts for hydrogen evolution reaction based on 2D MXenes. Journal of Energy Chemistry 2021; 55: 244-255.
23. Bhat K, Karthik S, Nagaraja H-S. Performance evaluation of molybdenum dichalcogenide (MoX2; X= S, Se, Te) nanostructures for hydrogen evolution reaction. International Journal of Hydrogen Energy. 2019; 44: 17878-17886.
24. Wang D, et al. Co-doped Mo2C/C hybrid electrocatalysts for improved hydrogen generation. Carbon 2018; 139: 845–852.
25. Lan K, et al. Nitrogen and phosphorus dual-doping carbon shells encapsulating ultrafine Mo2C particles as electrocatalyst for hydrogen evolution. J. Colloid Interfaces Sci. 2019; 553: 148–155.
26. Li J, et al. Confined Molybdenum Phosphide in P-Doped Porous Carbon as Efficient Electrocatalysts for Hydrogen Evolution, ACS Appl. Mater. Interfaces. 2018; 10: 17140–17146.
27. Hu Z, et al. Wrinkled Ni-doped Mo2C coating on carbon fiber paper: An advanced electrocatalyst prepared by molten-salt method for hydrogen evolution reaction. Electrochim. Acta 2019; 319: 293–301.
28. Zhang Y, et al. Molybdenum oxide and molybdenum carbide coated carbon black as an electrocatalyst for hydrogen evolution reaction in acidic media. Int. J. Hydrogen Energy 2017; 42: 26985–26994.

29. Song Y, et al. Facile synthesis of Mo2C nanoparticles on N-doped carbon nanotubes with enhanced electrocatalytic activity for hydrogen evolution and oxygen reduction reactions. J. Energy Chem. 2019; 38: 68–77.
30. Li X, et al. MoO_2 nanoparticles on reduced graphene oxide/polyimide-carbon nanotube film as efficient hydrogen evolution electrocatalyst. J. Power Sources. 2016; 304: 146–154.
31. Anjum M-A-R, et al. Sulfur and Nitrogen Dual-Doped Molybdenum Phosphide Nanocrystallites as an Active and Stable Hydrogen Evolution Reaction Electrocatalyst in Acidic and Alkaline Media. ACS Catal. 2021; 7: 3030–3038.
32. Wang M, et al. MoS_2/Co9S8/MoC heterostructure connected by carbon nanotubes as electrocatalyst for efficient hydrogen evolution reaction. J. Mater. Sci. Technol. 2021; 79: 29–34.
33. Wang D, et al. In Situ Preparation of Mo2C Nanoparticles Embedded in Ketjenblack Carbon as Highly Efficient Electrocatalysts for Hydrogen Evolution. ACS Sustain. Chem. Eng. 2018; 6: 983–990.
34. Xing J. Molybdenum carbide in-situ embedded into carbon nanosheets as efficient bifunctional electrocatalysts for overall water splitting. Electrochim. Acta 2019; 298: 305–312.
35. Zhang L, et al. Nanohybrid of Carbon Quantum Dots/Molybdenum Phosphide Nanoparticle for Efficient Electrochemical Hydrogen Evolution in Alkaline Medium. ACS Appl. Mater. Interfaces 2018; 10: 9460–9467.
36. Liu X, et al. Paragenesis of Mo_2C nanocrystals in mesoporous carbon nanofibers for electrocatalytic hydrogen evolution. Electrochim. Acta 2018; 274: 23–30.
37. Zhang L, et al. MoP/Mo_2C@C: A New Combination of Electrocatalysts for Highly Efficient Hydrogen Evolution over the Entire pH Range. ACS Appl. Mater. Interfaces 2017; 9: 16270–16279.
38. Adam A. Rationally dispersed molybdenum phosphide on carbon nanotubes for the hydrogen evolution reaction. ACS Sustain. Chem. Eng. 2018; 6: 11414–11423.
39. Adam A, et al. Controlled growth of small and uniformly dispersed Mo2C on carbon nanotubes as high performance electrocatalyst for the hydrogen evolution reaction. Int. J. Hydrogen Energy 2019; 44: 11797–11807.

40. Lin H, et al. Heteronanowires of MoC–Mo2C as efficient electrocatalysts for hydrogen evolution reaction. Chem. Sci. 2016; 7: 3399–3405.
41. Li J-S, et al. Coupled molybdenum carbide and reduced graphene oxide electrocatalysts for efficient hydrogen evolution. Nat. Commun. 2016; 7: 11204.
42. Yang XJ, et al. N-doped Graphene-Coated Molybdenum Carbide Nanoparticles as High Efficient Electrocatalyst for Hydrogen Evolution Reaction. J. Mater. Chem. A 2016; 4: 3947–3954.
43. Zheng Y, et al., Advancing the Electrochemistry of the Hydrogen-Evolution Reaction through Combining Experiment and Theory, Angew. Chem. Int. Ed., 54 (2015) 52–65.
44. T. Y. Ma, et al. Metal–Organic Framework Derived Hybrid Co3O4 -Carbon Porous Nanowire Arrays as Reversible Oxygen Evolution Electrodes. J. Am. Chem. Soc. 2014; 136: 13925–13931.
45. Zhao W-J, et al. Rod-like nonstoichiometric Ni0.85Se as efficient electrocatalysts for hydrogen evolution reaction, Int. J. Hydrogen Energy, 43 (2018) 12653–12660.
46. Chi J, et al. Heterointerface engineering of trilayer-shelled ultrathin MoS_2/MoP/N-doped carbon hollow nanobubbles for efficient hydrogen evolution. J. Mater. Chem. A 2018; 6: 24783–24792.
47. Li M-X, et al., Ni strongly coupled with Mo2C encapsulated in nitrogen-doped carbon nanofibers as robust bifunctional catalyst for overall water splitting. Adv. Energy Mater. 2019; 9: 1803185–1803196.
48. Xiong K, et al. Ni-doped Mo2C nanowires supported on Ni foam as a binder-free electrode for enhancing the hydrogen evolution performance. J. Mater. Chem. A 2015; 3: 1863–1867.
49. Wang B. Electron-transfer enhanced MoO_2 -Ni heterostructures as a highly efficient pH-universal catalyst for hydrogen evolution. Sci. China Chem. 2020; 63: 841–849.
50. Chi J. Heterointerface engineering of trilayer-shelled ultrathin MoS2/MoP/N-doped carbon hollow nanobubbles for efficient hydrogen evolution. J. Mater. Chem. A 2018; 6: 24783–24792.
51. Li M-X, et al. Ni strongly coupled with Mo2C encapsulated in nitrogen-doped carbon nanofibers as robust bifunctional catalyst for overall water splitting. Adv. Energy Mater. 2019; 9: 1803185–1803196.

52. Liu X, et al. Upraising the O 2p Orbital by Integrating Ni with MoO2 for Accelerating Hydrogen Evolution Kinetics. ACS Catal. 2019; 9: 2275–2285.
53. Yang X, et al. Rugae-like FeP nanocrystal assembly on a carbon cloth: An exceptionally efficient and stable cathode for hydrogen evolution. Nanoscale 2015; 7: 10974–10981.
54. Xu B, et al. Novel $Ni(S0.49Se0.51)_2$ porous flakes array on carbon fiber cloth for efficient hydrogen evolution reaction. Int. J. Hydrogen Energy. 2017; 42: 30119–30125.
55. Bukola S, et al. Nanostructured cobalt-modified molybdenum carbides electrocatalysts for hydrogen evolution reaction. Int. J. Hydrogen Energy 2016; 41: 22899–22912.
56. Lokhande PE, Pakdel A et al., Prospects of MXenes in energy storage applications. Chemosphere 2022; 297: 134225.
57. Kang Rui Garrick Lim, Albertus D. Handoko, et al., 2H-MoS_2 on Mo_2CT_x MXene Nanohybrid for Efficient and Durable Electrocatalytic Hydrogen Evolution. ACS Nano 2020; 14: 16140–16155.
58. Zhi Wei Seh, Kurt D. Fredrickson, et al., Two-Dimensional Molybdenum Carbide (MXene) as an Efficient Electrocatalyst for Hydrogen Evolution. ACS Energy Lett. 2016; 1: 589–594.
59. Albertus D. Handoko, Kurt D. Fredrickson et al., Tuning the Basal Plane Functionalization of Two-Dimensional Metal Carbides (MXenes) To Control Hydrogen Evolution Activity. ACS Appl. Energy Mater. 2018; 1: 173–180.
60. Chen N, et al. Heterostructured MoC-MoP/N-doped carbon nanofibers as efficient electrocatalysts for hydrogen evolution reaction. Electrochim. Acta 2019; 299: 708–716.
61. Fan X, et al. Atomic H-Induced Mo2C Hybrid as an Active and Stable Bifunctional Electrocatalyst. ACS Nano 2017; 11: 384–394.
62. An K, Xu X, Mo_2C based electrocatalyst with nitrogen doped three-dimensional mesoporous carbon as matrix, synthesis and HER activity study. Electrochim. Acta 2019; 293: 348–355.
63. Qamar M, et al. Metal–organic framework-guided growth of Mo_2C embedded in mesoporous carbon as a highperformance and stable electrocatalyst for the hydrogen evolution reaction. J. Mater. Chem. 2016; A 4: 16225–16232.

64. Xu B, et al. Facile and large-scale preparation of Co/Ni-MoO_2 composite as high-performance electrocatalyst for hydrogen evolution reaction. Int. J. Hydrogen Energy 2018; 43: 20721–20726.
65. Jian C, et al. Surface electron state engineering enhanced hydrogen evolution of hierarchical molybdenum disulfide in acidic and alkaline media. Appl. Catal. B Environ. 2020; 266: 118649.
66. Jiao Y. Porous Plate-like MoP Assembly as an Efficient pH-Universal Hydrogen Evolution Electrocatalyst. ACS Appl. Mater. Interfaces 2020; 12: 49596–49606.
67. Zhao D, et al. Synergistically Interactive Pyridinic-N–MoP Sites: Identified Active Centers for Enhanced Hydrogen Evolution in Alkaline Solution, Angew. Chem. Int. Ed., 2020; 2: 8982–8990.
68. Zhao H, et al. Heterostructured CoP/MoO_2 on Mo foil as high-efficiency electrocatalysts for the hydrogen evolution reaction in both acidic and alkaline media. J. Mater. Chem. A 2020; 8: 6732–6739.
69. Huang Y, et al. Hard template strategy for the synthesis of porous MoS2/MoO2 hybrid electrocatalyst for hydrogen evolution reaction. Appl. Surf. Sci. 2020; 520: 146340.
70. Qiufang G, et al. Ultrasmall and phase-pure W_2C nanoparticles for efficient electrocatalytic and photoelectrochemical hydrogen evolution. Nat. Commu. 2016; 7: 1-8.
71. Hussain S, et al. Pot Synthesis of W_2C/WS_2 Hybrid Nanostructures for Improved Hydrogen Evolution Reactions and Supercapacitors. Nanomaterials 2020; 10: 1597.
72. Fan X, et al. Wc nanocrystals grown on vertically aligned carbon nanotubes: An efficient and stable electrocatalyst for hydrogen evolution reaction. ACS Nano 2015; 9: 5125–5134.
73. Xu K, et al. Component-controllable WS2(1–x)Se2x nanotubes for efficient hydrogen evolution reaction. ACS Nano 2014; 8: 8468–8476.
74. Ma L, Efficient hydrogen evolution reaction catalyzed by molybdenum carbide and molybdenum nitride nanocatalysts synthesized via the urea glass route. J. Mater. Chem. A 2015; 3: 8361–8368.
75. Zhang K. Molybdenum carbide nanocrystal embedded n-doped carbon nanotubes as electrocatalysts for hydrogen generation. J. Mater. Chem. A 2015; 3: 5783–5788.
76. Li Y. Interface designing over WS2 /W2C for enhanced hydrogen evolution catalysis, *ACS* Appl. Energy Mater. 2018; 1: 3377–3384.

77. Nguyen TP. Facile synthesis of W2C@WS2 alloy nanoflowers and their hydrogen generation performance. Appl. Surf. Sci. 2020; 504: 144389.
78. Vikraman D, et al. Fabrication of MoS_2 /WSe2 heterostructures as electrocatalyst for enhanced hydrogen evolution reaction. Appl. Surf. Sci. 2019; 480: 611–620.
79. Vikraman D, et al. Improved hydrogen evolution reaction performance using MoS2–WS2 heterostructures by physicochemical process. ACS Sustain. Chem. Eng. 2018; 6: 8400–8409.
80. Li Y, et al. MoS_2 nanoparticles grown on graphene: An advanced catalyst for the hydrogen evolution reaction. J. Am. Chem. Soc. 2011; 133: 7296–7299.
81. Zhang K, et al. Porous one-dimensional Mo_2C–amorphous carbon composites: High-efficient and durable electrocatalysts for hydrogen generation. Phys. Chem. Chem. Phys. 2015; 17: 16609–16614.
82. Xu K, et al. Component-controllable $WS_2(1–x)Se_2x$ nanotubes for efficient hydrogen evolution reaction. ACS Nano 2014; 8: 8468–8476.
83. Šljuki´c B, et al. Carbon-supported Mo2C electrocatalysts for hydrogen evolution reaction, J. Mater. Chem. A 2015; 3: 15505–15512
84. Angel T, et al. Tungsten Carbide Nanoparticles as Efficient Cocatalysts for Photocatalytic Overall Water Splitting. ChemSusChem 2013; 6: 168–181
85. Hunt ST, et al. Engineering Non-sintered, Metal-Terminated Tungsten Carbide Nanoparticles for Catalysis. Angew. Chem. Int. Ed. 2014; 53: 5131 –5136.
86. Esposito DV, et al. A New Class of Electrocatalysts for Hydrogen Production from Water Electrolysis: Metal Monolayers Supported on Low-Cost Transition Metal Carbides. J. Am. Chem. Soc. 2012; 134: 3025–3033.
87. Ham DJ, et al. Tungsten carbide microsphere as an electrode for cathodic hydrogen evolution from water. International Journal of Hydrogen Energy 2008; 33: 6865-6872.
88. Rakoˇcevi´c L, Aleksandar Maksi´ et al., Hydrogen Evolution on Reduced Graphene Oxide-Supported PdAu Nanoparticles. Catalysts 2021; 11: 1-12.
89. Rakoˇcevi´c L. Hydrogen evolution on Au/GC and PdAu/GC nanostructures in acid solution: AFM, XPS, and electrochemical study. Int. J. Hydrog. Energy 2021; 46: 9052–9063.

90. Suffredini H-B, et al. The water decomposition reactions on boron-doped diamond electrodes. J. Braz. Chem. Soc. 2004; 15: 16–21.
91. Darabdhara G, et al. Reduced graphene oxide nanosheets decorated with Au, Pd and Au-Pd bimetallic nanoparticles as highly efficient catalysts for electrochemical hydrogen generation. J. Mater. Chem. A 2015; 3: 20254–20266.
92. Ferrari A-G-M, et al. Investigating the integrity of graphene towards the electrochemical hydrogen evolution reaction (HER). Sci. Rep. 2019; 9: 15961.
93. Ghasemi S. Palladium nanoparticles supported on graphene as an efficient electrocatalyst for hydrogen evolution reaction. Int. J. Hydrog. Energy 2015; 40: 16184–16191.
94. Ito Y. High catalytic activity of nitrogen and sulfur co-doped nanoporous graphene in the hydrogen evolution reaction. Chem. Int. Ed. 2014; 53: 1–7.
95. Rakoˇcevi´c L, et al. Hydrogen evolution on Au/GC and PdAu/GC nanostructures in acid solution: AFM, XPS, and electrochemical study. Int. J. Hydrog. Energy 2021; 46: 9052–9063.
96. Smiljani´c M, et al. Catalysis of hydrogen evolution on Au(111) modified by spontaneously deposited Pd islands. Electrocatalysis 2012; 3: 369–375.
97. Wang Y, et al. Activation effect of electrochemical cycling on gold nanoparticles towards the hydrogen evolution reaction in sulfuric acid. Electrochim. Acta 2016; 209: 440–447.
98. Feng JJ, et al. Bimetallic AuPd nanoclusters supported on graphitic carbon nitride: One-pot synthesis and enhanced electrocatalysis for oxygen reduction and hydrogen evolution. Int. J. Hydrog. Energy 2016; 41: 8839–8846.
99. Shinagava T, et al. Insight on Tafel slopes from a microkinetic analysis of aqueous electrocatalysis for energy conversion. Sci. Rep. 2015; 5: 13801.
100. Feng JJ, et al. Bimetallic AuPd nanoclusters supported on graphitic carbon nitride: One-pot synthesis and enhanced electrocatalysis for oxygen reduction and hydrogen evolution. Int. J. Hydrog. Energy 2016; 41: 8839–8846.
101. Li D-N. Facile synthesis of flower-like Au@AuPd nanocrystals with highly electrocatalytic activity for formic acid oxidation and hydrogen evolution reactions. Int. J. Hydrog. Energy 2017; 42: 19894–19902.
102. Santos JL. Bimetallic PdAu catalysts for formic acid dehydrogenation, Int. J. Hydrog. Energy 2020; 45: 23056–23068.

103. Cheng W, et al., RuCo Alloy Nanoparticles Embedded into N-Doped Carbon for High Efficiency Hydrogen Evolution Electrocatalyst, Energies 2022; 15: 290.

104. Choi W, et al. Effects of metal-doping on hydrogen evolution reaction catalyzed by MAu24 and M2Au36 nanoclusters (M = Pt, Pd). ACS Appl. Mater. Interfaces 2018; 10: 44645–44653.

105. Tiwari JN, Ahmad MH et al. High-Performance Hydrogen Evolution by Ru Single Atoms and Nitrided-Ru Nanoparticles Implanted on N-Doped Graphitic Sheet, Adv. Energy Mater. 2019; 9: 1900931.

106. Johnston C-M, et al. In situ STM study of Au(111)/Os bimetallic surfaces: Spontaneous deposition and electrochemical dissolution. Langmuir 2005; 21: 9610–9617.

107. Wang C, et al. RuCo Alloy Nanoparticles Embedded into N-Doped Carbon for High Efficiency Hydrogen Evolution Electrocatalyst. Energies 2022; 15: 2908.

108. Sultan S, et al. Modulation of Cu and Rh single-atoms and nanoparticles for high-performance hydrogen evolution activity in acidic media, J. Mater. Chem. A 2021; 9**:** 10326-10334.

109. Wang H, et al. Significantly Enhanced Overall Water Splitting Performance by Partial Oxidation of Ir through Au Modification in Core-Shell Alloy Structure. J. Am. Chem. Soc. 2021; 143: 4639–4645.

110. Jiang X, et al. The Heterostructure of Ru2P/WO3/NPC Synergistically Promotes H2O Dissociation for Improved Hydrogen Evolution. Angew. Chem. Int. Ed. Engl. 2021; 60: 4110–4116.

111. Zhang F, et al. RuCo alloy bimodal nanoparticles embedded in N-doped carbon: A superior pH-universal electrocatalyst outperforms benchmark Pt for the hydrogen evolution reaction. J. Mater. Chem. A 2020; 8: 12810–12820.

112. Kumar S-S. Phosphorus-doped graphene supported palladium (Pd/PG) electrocatalyst for the hydrogen evolution reaction. Int. J. Green Energy 2018; 15: 558–567.

113. Brito J, et al. Implementation of Transition Metal Phosphides as Pt-Free Catalysts for PEM Water Electrolysis. Energies 2022; 15: 1821.

114. Wang J, et al. Engineering the Composition and Structure of Bimetallic Au–Cu Alloy Nanoparticles in Carbon Nanofibers: Self-Supported Electrode Materials for Electrocatalytic Water Splitting. ACS Appl. Mater. Interfaces 2017; 9: 19756–19765.

115. Zhong X, et al. Integrating cobalt phosphide and cobalt nitride-embedded nitrogen-rich nanocarbons: High-performance bifunctional electrocatalysts for oxygen reduction and evolution. J. Mater. Chem. A 2016; 4: 10575–10584.

116. Xu Y, et al., Low-ruthenium-content NiRu nanoalloys encapsulated in nitrogen-doped carbon as highly efficient and pH-universal electrocatalysts for the hydrogen evolution reaction. J. Mater. Chem. A 2018; 6: 1376–1381.

117. Nørskov JK, Towards the computational design of solid catalysts. Nat. Chem., 2009; 1: 37–46.

118. Hammer B, et al., Electronic factors determining the reactivity of metal surfaces. Surface Science 1995; 343: 211–220.

119. Sun S. Tailoring the d-Band Centers Endows (NixFe1–x)2P Nanosheets with Efficient Oxygen Evolution Catalysis. ACS Catal. 2020; 10: 9086–9097.

120. Gou W, et al. Downshifted d-Band Center of Ru/MWCNTs by Turbostratic Carbon Nitride for Efficient and Robust Hydrogen Evolution in Alkali. ChemCatChem 2019; 11: 1970–1976.

121. Ha, M. et al., Tuning metal single atoms embedded in N_xC_y moieties toward high-performance electrocatalysis, Energy Environ. Sci 2021; 14: 3455-3468

122. Umer, M. et al., Machine learning assisted high-throughput screening of transition metal single atom based superb hydrogen evolution electrocatalysts. J Mater Chem A 2022; 10: 6679.

123. Dang NK, Umer M, et al., Surface enrichment of iridium on IrCo alloys for boosting hydrogen production, J. Mater. Chem. A**,** 2021; 9**:** 16898-16905

124. Qazi UY, Future of Hydrogen as an Alternative Fuel for Next-Generation Industrial Applications; Challenges and Expected Opportunities. Energies 2022; 15: 1-40.

125. Sukanya R, et al., Review—Recent Developments in the Applications of 2D Transition Metal Dichalcogenides as Electrocatalysts in the Generation of Hydrogen for Renewable Energy Conversion, Journal of The Electrochemical Society 2022; 169: 064504.